

## Characterization of Calcium in Hydroxyapatite by an XAFS Method

T. Kurisaki<sup>1</sup>, Y. Nagino<sup>1</sup>, S. Yokoyama<sup>1</sup> and H. Wakita<sup>1,2</sup>

<sup>1</sup>Department of Chemistry, Faculty of Science, Fukuoka University, Nanakuma, Jonan-ku, Fukuoka 814-0180, Japan

<sup>2</sup>Advanced Materials Institute, Fukuoka University, Nanakuma, Jonan-ku, Fukuoka 814-0180, Japan

Hydroxyapatite is a kind of calcium phosphate. This compound can be found in tooth and born in the human body. In addition, it is commonly used as a filler to replace amputated born or as a coating to promote bone ingrowth into prosthetic implants. However, the local structure and electronic structure of calcium in a tooth and hydroxyapatite (HAP) are not determined. For various light element compounds, we have studied the electronic structure by X-ray absorption spectroscopy [1]. These results suggested that there is a correlation between XANES spectra and the local structures.

In this work, we performed the XANES spectra measurement about tooth, decayed tooth and hydroxyapatite. The obtained experimental XANES spectra are analyzed using the calculated theoretical spectra from DV-X $\alpha$  calculations. The X-ray absorption spectra were measured at BL2A of the UVSOR in the Institute of Molecular Science, Okazaki [2]. The ring energy of the UVSOR storage ring was 750MeV. Ca K-edge absorption spectra were recorded in the regions of 4000-4200eV by use of two InSb crystals. The absorption was monitored by the total electron yield using a photomultiplier.

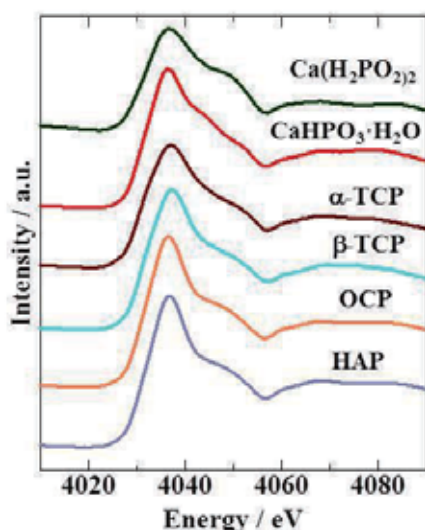


Fig. 1. Ca K-edge XANES spectra of the calcium phosphate compounds.

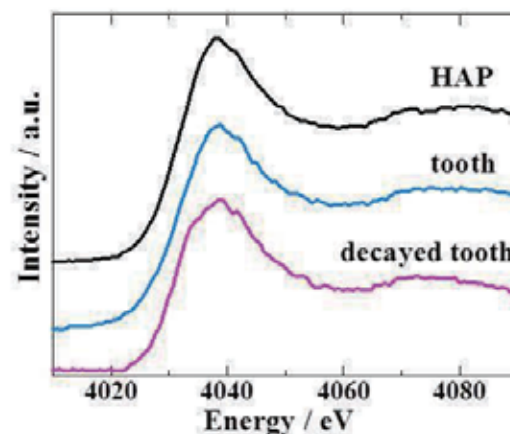


Fig. 2. Ca K-edge XANES spectra of the HAP, tooth and decayed tooth.

The samples were spread onto the carbon tape on the first photodynode made of CuBe of the photomultiplier.

Figure 1 shows the observed Ca K-edge XANES spectra for the calcium phosphate compounds. This result suggested that the measured Ca K-edge XANES spectra shows different peak profiles depending on the electronic structure and local structure of the these compounds.

Figure 2 shows the observed Ca K-edge XANES spectra for the HAP, tooth and decayed tooth. The Ca K-edge XANES spectra of HAP and tooth show the same peak profiles. On the other hand, the Ca K-edge XANES spectra of decayed tooth show a little difference of the peak profiles at 4037eV in comparison with the Ca K-edge XANES spectra of HAP and tooth. These results indicated that the electronic structure and local structure around the calcium in decayed tooth is different from those of HAP and tooth.

[1] T. Kurisaki S. Matsuo, I. Toth and H. Wakita, *Anal. Sci.* **24** (2008) 1385.

[2] S. Murata, T. Matsukawa, S. Naoè, T. Horigome, O. Matsuodo and M. Watatabe, *Rev. Sci. Instrum.* **63** (1992) 1309.

## Defects in Metal Oxide Studied by X-ray Absorption Fine Structure Spectroscopy

E. Kobayashi<sup>1</sup>, K. K. Bando<sup>2</sup> and T. Okajima<sup>1,3</sup>

<sup>1</sup>*Kyushu Synchrotron Light Research Center, 8-7 Yayoiogaoka, Tosu, Saga 841-0005, Japan*

<sup>2</sup>*National Institute of Advanced Industrial Science and Technology, 1-1-1, Higashi, Tsukuba, Ibaraki 305-8565, Japan*

<sup>3</sup>*Research Center for Synchrotron light applications, Kyushu University, 6-1 Kasugakoen, Kasuga, Fukuoka 816-8580, Japan*

Metal oxide is an important material from a fundamental physical point of view and is widely used in the field of catalytic, optical and electrical applications. It is recognized that the defects in metal oxide is important for applications because it can significantly affect the material characteristics. To understanding of the character of the defects is of importance for the development of new materials.

MgO plays a prototype of metal oxides and is also a wide-gap insulator [1]. The important defects in MgO are oxygen vacancies. We have investigated the MgO surface defects induced by ion bombardment in metal oxide. In this study, the annealing behavior of hydrogen defects of MgO bulk was studied by Mg *K*-edge NEXAFS spectroscopy using fluorescence yield (FY) method.

X-ray absorption fine structure spectra in the soft X-ray region can be obtained by detecting either the electrons or the fluorescence. For insulating materials, the total electron yield (TEY) method cannot be used due to the charge up. The FY can be measured for metal oxide, but the intensity is very low in the soft x-ray region, this is sensitive to the bulk material whereas the TEY is surface-sensitive.

The samples were MgO pellets after annealing at 673 K ~ 1073 K for 2 hours in hydrogen atmosphere and MgO reference powder. NEXAFS spectra were measured at the beamline 2A of the UVSOR in the Institute of Molecular Science. The NEXAFS spectra were obtained by measuring the fluorescence from the sample. The incident angle of the synchrotron radiation was 0° from the surface normal. The FY was normalized to the incident photon flux, recorded as a photocurrent at a photon-flux monitor consisting of a gold-evaporated mesh.

Figure 1 shows the NEXAFS spectra for the Mg *K*-edge region of MgO pellets after annealing at 673 K ~ 1073 K for 2 hours in hydrogen atmosphere and MgO reference powder. Three strong peaks are observed at around 1309.1 eV, 1314.7 eV and 1316.9 eV, respectively. The spectrum exhibits an overall similarity with those previously obtained by experiments [2]. The edge of the spectrum is shifted by annealing under a hydrogen atmosphere. This indicates that the hydrogen reduction of MgO was carried out. The oxygen of MgO is reduced by the hydrogen, the edge is shifted to the low energy.

After the hydrogen reduction, the strongest peaks become broad peak. In addition, the intensity of the peaks decreases with increasing temperature. These results indicate that the oxygen vacancies were induced by hydrogen reduction and the amorphous phase increased with annealing.

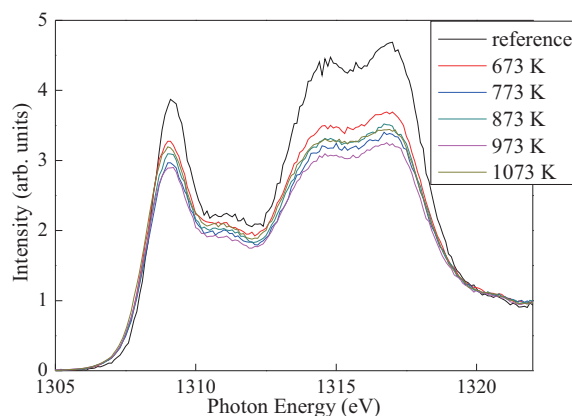


Fig. 1. NEXAFS spectra for the Mg *K*-edge region of MgO pellets after annealing at 673 K ~ 1073 K for 2 hours in hydrogen atmosphere and MgO reference powder.

[1] D. M. Roessler and W. C. Walker, *Phys. Rev.* **159** (1967) 733.

[2] P. Luches, S. D'Addato, and S. Valeri, E. Groppo, C. Prestipino and C. Lamberti, F. Boscherini, *Phys. Rev. B* **69** (2004) 045412.

## Ultraviolet Emission of AlGdN by Inner-Core Excitation

K. Fujita, R. Ikematsu and K. Fukui

Department of Electrical and Electronics Engineering, University of Fukui, Fukui 910-8507, Japan

III-V nitride compound semiconductors doped with rare earth (RE) elements are attractive systems because of the possibility of magnetic ordering coupled with a semiconducting natures and luminescence properties, so-called spintronics. However, even in light emitter the III-V nitride wide band-gap host materials with REs have potential for development. In the case of ultraviolet (UV) region where is used as sterilization lamp and excitation lamp for phosphors in the visible region,  $Gd^{3+}$  is known as the light emitting material having  $\sim 3.9$  eV emission (UVE) by  ${}^6P_{7/2} \rightarrow {}^8S_{7/2}$   $4f$  intra-transition of  $Gd^{3+}$ . Since the UVE is higher than the band-gap energy of the GaN (3.4 eV), the realistic host materials are AlGa<sub>N</sub> or AlN. In our previous work [1], we studied photoluminescence (PL) and PL excitation (PLE) spectra of AlN doped with  $Gd^{3+}$  in the band-to-band excitation region. A sharp line of the UVE was clearly observed, and its PLE spectra revealed that this emission process is host excitation. It means that there is a process which transfers energy from the band-to-band excitation of AlN to  $4f$  intra-transition of  $Gd^{3+}$  ion, and also means that UVE does not observed if the excitation light photon energy is less than that of AlN bandgap. Then, we have performed the ultraviolet (UV) emission of AlGdN thin films by Al 1s and Gd 3d core excitations to investigate the emission process of AlGdN.

AlGdN thin films were grown in a MBE system with a RF-plasma assisted radical cell on the Si-face of (0001)-oriented 6H-SiC substrates. The thickness of the sample is about 120 nm. Concentration of  $Gd^{3+}$  ions are 2 % ( $Al_{0.98}Gd_{0.02}N$ ) and 13 % ( $Al_{0.87}Gd_{0.13}N$ ). The details of the crystal growth have been reported elsewhere [2]. All visible (VIS) – UV region photoluminescence (PL) measurements were carried out at  $\sim 20$  K with a conventional 30 cm VIS – UV monochromator and CCD image detector. PL excitation (PLE) and total yield (TY) spectra were measured around both Al K-edge ( $\sim 1.5$  keV) and Gd  $M_{IV}$ -edge ( $\sim 1.2$  keV). TY measurements were carried out at RT.

Figure 1 shows the PL spectrum of  $Al_{0.98}Gd_{0.02}N$ . The excitation energy is 1569 eV. A sharp line of the UVE is observed. Figures 2(a) and 2(b) show the TY and the PLE spectrum of  $Al_{0.98}Gd_{0.02}N$ , respectively. The intensity of the PLE spectrum is integrated intensity of the UVE shown in fig. 1. Both TY and PLE spectra around Al K-edge in fig. 2 are in good agreements with TY spectrum of AlN [3]. Since TY spectrum in this energy region is similar to the absorption spectrum, these results are consistent with our previous works as mentioned above.

Figures 3(a) and 3(b) represent the TY and the PLE

spectrum of  $Al_{0.87}Gd_{0.13}N$ , respectively. These spectra of  $Al_{0.98}Gd_{0.02}N$  were not observed. Both TY and PLE spectra near Gd  $M_{IV}$ -edge are in good agreements with TY spectrum of  $Gd^{3+}$  ion which is well explained by the  $3d^{10}4f^7 \rightarrow 3d^9 4f^8$  transition array [4].

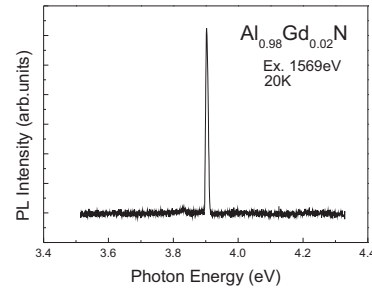


Fig. 1. PL spectrum of  $Al_{0.98}Gd_{0.02}N$

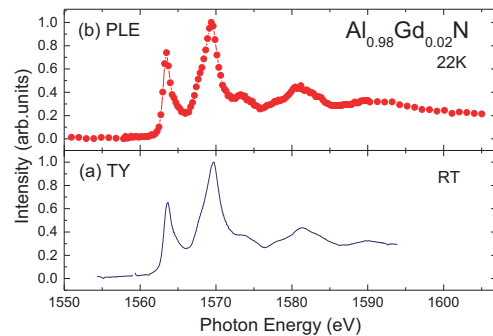


Fig. 2. TY (a) and PLE (b) spectra of  $Al_{0.98}Gd_{0.02}N$  around Al K edge.

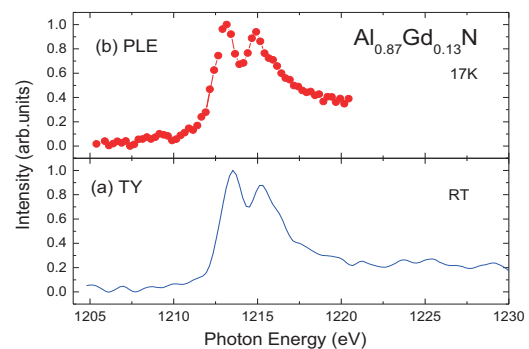


Fig. 3. TY (a) and PLE (b) spectra of  $Al_{0.87}Gd_{0.13}N$  around Gd  $M_{IV}$  edge.

- [1] K. Fukui *et al.*, Phys. Stat. Sol. (c) **7** (2010) 1878.
- [2] N. Teraguchi *et al.*, J. Cryst. Growth **230** (2001) 392.
- [3] K. Fukui *et al.*, Phys. Stat. Sol. (b) **228** (2001) 461.
- [4] C. Bonnelle *et al.*, J. Phys. B **10** (1977) 795.

## Optical Spectra of NaCl:Ag<sup>-</sup> Crystals up to the VUV Energy Region

T. Kawai<sup>1</sup>, T. Hirai<sup>2</sup> and K. Bando<sup>3</sup>

<sup>1</sup>Graduate School of Science, Osaka Prefecture University, Sakai 599-8531, Japan

<sup>2</sup>Faculty of Science and Engineering, Ritsumeikan University, Kusatsu 525-8577, Japan

<sup>3</sup>Faculty of Science, Shizuoka University, Shizuoka 422-8529, Japan

Ag<sup>-</sup> ions belong to the family of the so-called TI<sup>+</sup>-type ions and exhibit the optical bands called A, B, and C [1, 2]. In alkali halide crystals doped with the TI<sup>+</sup>-type ions, the absorption bands labeled D are often observed in the energy region between the C band and the fundamental absorption edge of the host crystals [3]. However, the existence of the D bands has not been reported for the Ag<sup>-</sup> centers in alkali halides. In this study, optical spectra of NaCl:Ag<sup>-</sup> crystals have been investigated in the energy region between the C absorption band and the fundamental absorption edge.

NaCl:Ag<sup>+</sup> crystals were grown by the Bridgman method from the NaCl powders containing the AgCl concentration of 0.01 mol%, which corresponds to the Ag<sup>+</sup> ion concentration of about  $2.3 \times 10^{18}$  number/cm<sup>3</sup> in the crystal. The conversion from the Ag<sup>+</sup> to Ag<sup>-</sup> ions in the crystals was achieved by an electrolytic coloration technique. The optical measurements were performed at the BL-3B of UVSOR.

Figure 1 shows the absorption spectra of NaCl:Ag<sup>+</sup> and NaCl:Ag<sup>-</sup> crystals. In NaCl:Ag<sup>+</sup>, an absorption band peaking at 6.9 eV and the steep rise from 7.2 eV can be seen. The absorption band at 6.9 eV is attributed to the partially-allowed transition of  $4d^{10} \rightarrow 4d^95s$  in the Ag<sup>+</sup> ion. The steep rise from 7.2 eV corresponds to the lower tail of the absorption band due to an electronically allowed transition in the Ag<sup>+</sup> ion [4].

In NaCl:Ag<sup>-</sup>, the absorption band at 6.9 eV disappears and the steep rise from 7.2 eV shifts to the higher energy side. The C absorption band due to the Ag<sup>-</sup> centers is obviously observed at 4.6 eV [2]. The fact implies that the Ag<sup>+</sup> ions are efficiently transformed to the Ag<sup>-</sup> ions by the electrolytic coloration. In addition to the C absorption band, the intense and small absorption bands are observed at 6.51 and 7.10 eV, respectively.

Figure 2 shows the excitation spectra for the A' and C' luminescence bands due to the Ag<sup>-</sup> centers, which are shown in the insert of Fig. 2. The C' luminescence band is efficiently excited at around 6.9 eV corresponding to the C absorption band. The A' luminescence band is excited at the higher energy region in the C absorption band. It should be noted that the excitation spectrum for the A' luminescence has the peaks at 7.10 and 7.60 eV. The peak energy of 7.10 eV is equal to that of the small absorption band of NaCl:Ag<sup>-</sup>, as shown in Fig. 1. Thus, the small absorption band at 7.1 eV will be related to the Ag<sup>-</sup>

centers and might be assigned to the D band. On the other hand, both the A' and C' luminescence bands are not excited at around 6.5 eV, where the intense absorption band is located. This fact indicates that the 6.5 eV absorption band in NaCl:Ag<sup>-</sup> has no relationship with the Ag<sup>-</sup> centers. The 6.5 eV absorption band might be associated with the Ag<sup>0</sup> atoms which were not converted to the Ag<sup>-</sup> ions through the electrolytic coloration.

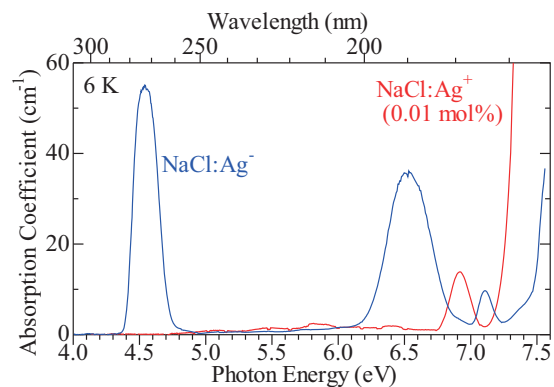


Fig. 1. Absorption spectra of NaCl:Ag<sup>+</sup> (red) and NaCl:Ag<sup>-</sup> (blue) crystals.

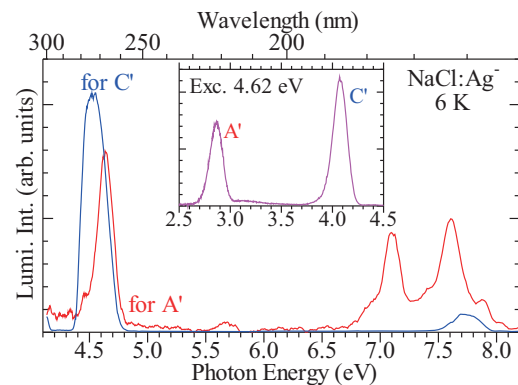


Fig. 2. Excitation spectra for the A' (red) and C' (blue) luminescence bands. Insert is the luminescence spectrum under excitation at 4.62 eV

- [1] W. Kleemann, Z. Physik **234** (1970) 362.
- [2] S. Shimanuki, J. Phys. Soc. Jpn. **35** (1973) 1680.
- [3] A. Ranfagni *et al.*, Advances in Physics **32** (1983) 823.
- [4] R. Onaka *et al.*, Jpn. J. Appl. Phys. **4** (1965) Suppl.1, 631.

## Experimental Evidence for Migration and Trapping of Excited Electrons in Ce:Gd<sub>3</sub>(Al,Ga)<sub>5</sub>O<sub>12</sub> Single Crystals

A. Satoh<sup>1</sup>, M. Kitaura<sup>1</sup>, K. Kamada<sup>2</sup>, A. Ohnishi<sup>1</sup> and M. Sasaki<sup>1</sup>

<sup>1</sup>Dept. of Physics, Faculty of Science, Yamagata University, 1-4-12 Kojirakawa, Yamagata 990-8560, Japan

<sup>2</sup>Materials laboratory of Furukawa Co. Ltd, 1-25-13 Kannondai, Tsukuba 305-0856, Japan

Rare-earth doped A<sub>3</sub>B<sub>5</sub>O<sub>12</sub> (A=Y, Lu, Gd; B=Sc, Al, Ga) garnet crystals attract much attention as a material group of inorganic scintillators useful for x- and  $\gamma$ -ray detection. Scintillation properties of this group have been remarkably improved by the combination of band-gap engineering and rare-earth 5d level positioning strategies [1, 2]. By such great efforts, a novel Ce<sup>3+</sup> doped Gd<sub>3</sub>(Al,Ga)<sub>5</sub>O<sub>12</sub> (Ce:GAGG) scintillator crystal has been recently developed [3]. Further improvement of crystal quality is necessary in order to meet the demand for the application into various scientific and industrial fields. For this purpose, it is expected that spectroscopy experiment bring valuable information. In the present study, we have measured absorption spectra and excitation spectra of the 2.34 eV emission band due to 5d - 4f transitions of Ce<sup>3+</sup> ions at various temperatures, in order to clarify migration and trapping processes of photo-carriers in GAGG crystals. Crystals of Ce:GAGG and GAGG were grown in Ar + O<sub>2</sub> (2%) atmosphere from melt by the Czochralski method. Experiment was performed at the BL3B beam line of UVSOR. The absorption and excitation spectra measured were corrected with a calibrated silicon photodiode sensor for the distribution of an excitation light.

Figure 1 shows absorption spectra of a Ce:GAGG single crystals observed at 6 K and 300 K. The concentration of Ce<sup>3+</sup> ions in the Ce:GAGG crystal was determined to 0.08 mol%. The absorption spectra exhibit broad bands at 2.82 eV and 3.62 eV, and narrow lines around 4 - 5 eV. The broad bands appear by the incorporation of Ce<sup>3+</sup> ions, and they are thus assigned to the 4f - 5d transitions of Ce<sup>3+</sup> ions. The narrow lines were observed in absorption spectra of GAGG single crystals. We connect these lines to the 4f - 4f transitions of Gd<sup>3+</sup> ions. The absorption coefficient is abruptly increased in the photon energy range from 5.75 to 6 eV. This is due to the fundamental absorption edge of the host GAGG crystal, the photon energy of which is determined to be 5.96 eV at 6 K and 5.69 eV at 300 K.

Excitation spectra for the 2.34 eV emission band of Ce:GAGG (0.08 mol%) are shown in Fig. 2. The intensity of the 2.34 eV emission band does not almost depend on temperature under excitation in the lowest energy Ce<sup>3+</sup> 4f - 5d absorption band at 2.81 eV. In contrast, the intensity is varied with increasing temperature, when the crystal is excited in the energy region higher than 2.81 eV absorption peak. This result is explained as follows. At low temperature,

excited electrons are partially trapped at defect levels. With increasing temperature, trapped electrons are released from the defect levels via a thermal activation process, and they migrate to electron-lost Ce<sup>4+</sup> sites. The excited states of Ce<sup>3+</sup> ions are more increased, compared to those at low temperature, and the 2.34 eV emission band is thus enhanced. The origin of defects responsible for such an enhancement is now in investigation.

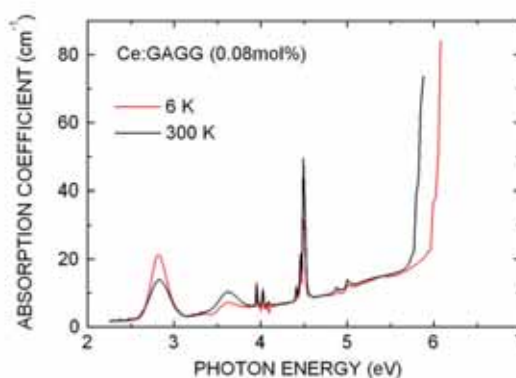


Fig. 1. Absorption spectra of a Ce:GAGG (0.08 mol%) single crystal observed at 6 K (red line) and 300 K (black line).

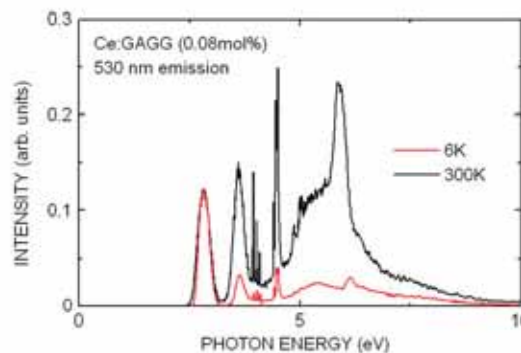


Fig. 2. Excitation spectra for the 2.34 eV emission band of a Ce:GAGG (0.08 mol%) single crystal, observed at 6 K (red line) and 300 K (black line).

- [1] K. Kamada *et al.*, Cryst. Growth & Des. **11** (2011) 4484.
- [2] M. Fasoli *et al.*, Phys. Rev. B **84** (2011) 081102(R).
- [3] K. Kamada *et al.*, J. Cryst. Growth **352** (2012) 88.

## Combined Excitation-Emission Spectroscopy of Boron-Doped Diamond Films

T. Toyoda<sup>1</sup>, K. Fukui<sup>1</sup> and T. Inushima<sup>2</sup>

<sup>1</sup>Department of Electrical and Electronics Engineering, University of Fukui, Fukui 910-8507, Japan

<sup>2</sup>Department of Electronics, Tokai University 4-1-1 Kitakaname, Hiratsuka 259-1292, Japan

Boron-doped diamond (BDD) is one of the p-type wide band-gap (5.5eV) semiconductors. Recently, the superconductivity has been discovered in heavily BDD [1]. In this study, we have measured the CEES (Combined Excitation Emission Spectroscopy) around the band-gap (excitation energy 4.5 ~ 7.0eV) in order to clarify the electron state of BDD whose boron concentrations is in the metal-semiconductor transition region.

The BDD films used in this study are grown on Ib-synthesized diamond substrates by the MPCVD (Microwave Plasma Chemical Vapor Deposition) method and their boron concentration are 1000, 2000, 5000 and 10000 ppm [2]. All CEES measurements including the diamond substrate (0 ppm) have been performed at BL3B.

Figure 1(A) and 1(B) show the CEES spectra at 9 K of the 1000 ppm and 10000 ppm BDDs, respectively. The horizontal axis represents the emission energy, and the vertical the excitation energy. A strong emission region around 2.4 eV (white color region in Fig. 1(A)) consists of two emission bands. One is shown at lower excitation energy side which has clear higher energy cut of the emission spectrum shape at 2.5 eV. This characteristic emission band is known as the band due to the H3 center (H3 band) which is nitrogen defect related center in diamond. In fact, the H3 band is clearly observed in diamond substrate (0 ppm) sample. The difference of the H3 band in between 0 ppm and 1000 ppm is the existence or nonexistence of the higher excitation energy limit, because there is no limit in the case of 0 ppm sample but about 6.0 eV in the case of 1000 ppm. The other emission band has a broad Gaussian like line shape and is observed at higher excitation energy side. The lower excitation energy limit is about 5.5 eV where is almost same energy as the indirect band-gap energy of the diamond. This emission band is often observed in the BDD and is considered donor-acceptor pair (DAP) emission (G band), where the acceptor is boron [3]. These results suggest that (i) the higher excitation energy side emission band is the G band of the BDD, (ii) the lower side band is H3 band of the diamond substrate, (iii) 1000 ppm BDD has the direct band-gap of ~ 6.0 eV.

In the case of the 10000 ppm BDD (fig. 1(B)), the strong regions clearly separate two regions. One is shown in the emission energy around 2.4 eV (white color region in fig. 1(B)). This band is H3 band of the diamond substrate as mentioned above. A new band around 2.8 eV (red color circle in fig. 1(B)) is

observed. The origin of this band is not clear at present, but it is clear that this emission is caused by the band to band excitation and there is no overlap of the excitation energy between this new band and the H3 band. These behaviors are consistent with the previous work [2, 4].

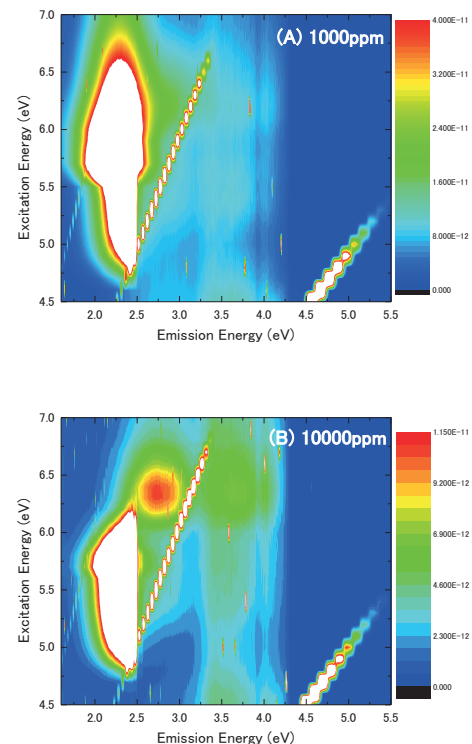


Fig. 1. CEES of BDD (A) 1000 ppm and (B) 10000 ppm at 9 K.

[1] E. A. Ekimov, V. A. Sidorov, E. D. Bauer, N. N. Mel'nik, N. J. Curro, J. D. Thompson and S. M. Stishov, *Nature* **428** (2004) 542.

[2] A. Ogasawara, T. Inushima, T. Shiraiishi, S. Ohya, S. Karasawa and H. Shiomi, *Diamond Relat. Mater.* **6** (1997) 835.

[3] E. Gaillou, Jeffrey E. Post, D. Rost and J. E. Butler, *Am. Mineral.* **97** (2012) 1.

[4] T. Inushima, Y. Ota, K. Fukui, *UVSOR Activity Report* **38** (2010) 101.

## Valence State Analysis of Mn Ions in $\text{In}_2\text{O}_3:(\text{Mn}, \text{TM})$ (TM = Cr, Fe, Co)

S. Nishida<sup>1</sup>, T. Yoshioka<sup>1</sup> and T. Yamamoto<sup>1,2</sup>

<sup>1</sup> Faculty of Science and Engineering, Waseda University, Tokyo 169-8555, Japan

<sup>2</sup> Institute of Condensed-Matter Science, Waseda University, Tokyo 169-8555, Japan

The dilute magnetic materials (DMMs) have been extensively studied through experiments and theoretical calculations [1, 2], which have ferromagnetic properties with dilute magnetic elements, because of the possibility of their future applications in spintronics. Although the Curie temperature of most DMMs were quite low, it was recently reported that some DMMs show room-temperature ferromagnetism [3, 4]. Among them, a sintered polycrystalline specimen of Mn- and Fe-codoped  $\text{In}_2\text{O}_3$  ( $\text{In}_2\text{O}_3:(\text{Mn}, \text{Fe})$ ) shows the property [4]. For a deeper understanding of the mechanism of ferromagnetism in  $\text{In}_2\text{O}_3:(\text{Mn}, \text{Fe})$ , substitution mechanism of magnetic elements was investigated, in which Mn and Fe ions are substituted at the In sites in  $\text{In}_2\text{O}_3$  [5]. In addition, it was found that the coexistence of  $\text{Mn}^{2+}$  and  $\text{Mn}^{3+}$  is mandatory for room-temperature ferromagnetism in  $\text{In}_2\text{O}_3:(\text{Mn}, \text{Fe})$  [6]. In the present study, the valence state analysis of doped Mn ions have been carried out using Mn-L<sub>3</sub> X-ray Absorption Near-Edge Structure (XANES) measurements in order to investigate the difference in electronic structure between ferromagnetic  $\text{In}_2\text{O}_3:(\text{Mn}, \text{Fe})$  and paramagnetic  $\text{In}_2\text{O}_3:(\text{Mn}, \text{Cr})$  and  $\text{In}_2\text{O}_3:(\text{Mn}, \text{Co})$ .

All polycrystalline specimens,  $\text{In}_2\text{O}_3:(\text{Mn}, \text{TM})$  ( $(\text{In}_{0.94}\text{Mn}_{0.03}\text{TM}_{0.03})_2\text{O}_3$ , TM=Cr, Fe, Co), were synthesized by the conventional solid-state reaction method. Mn-L<sub>3</sub> XANES spectra were collected at BL4B in UVSOR by the total electron yield (TEY) method. All the sample powders were mounted on the first Be-Cu dinode using the carbon adhesive tape. The incident beam was monochromatized by the varied-line-spacing plane grating (800 lines/mm). The energy resolution of the incident beams,  $E/\Delta E$  was set to 3000 by tuning the slit height settled at the upper and lower reaches of the grating.

Prior to the XANES analysis, all the samples were characterized by the X-ray diffraction (XRD). No extra peaks were found in these XRD patterns except for the peaks originating from the bixbyite-structured  $\text{In}_2\text{O}_3$ . Then all the samples were determined to be crystallized in a single-phased cubic bixbyite-structured (*Ia*3). The observed Mn-L<sub>3</sub> XANES spectra of  $\text{In}_2\text{O}_3:(\text{Mn}, \text{TM})$  are shown in Fig. 1, together with the reference spectra of  $\text{Mn}^{2+}$  (MnO) and  $\text{Mn}^{3+}$  ( $\text{Mn}_2\text{O}_3$ ). The profiles of the Mn-L<sub>3</sub> XANES spectra of  $\text{Mn}^{2+}$  (MnO) and  $\text{Mn}^{3+}$  ( $\text{Mn}_2\text{O}_3$ ) are clearly different and can be easily distinguished from the characteristic peak energies of their peaks. By comparing to these standard spectra of Mn oxides, the

observed Mn-L<sub>3</sub> XANES spectra of  $\text{In}_2\text{O}_3:(\text{Mn}, \text{Cr})$  and  $\text{In}_2\text{O}_3:(\text{Mn}, \text{Fe})$  can be determined to be a mixture of the spectra of  $\text{Mn}^{2+}$  and  $\text{Mn}^{3+}$ , on the other hand, that of  $\text{In}_2\text{O}_3:(\text{Mn}, \text{Co})$  can be determined to be  $\text{Mn}^{3+}$ .

Mn ions are trivalent in paramagnetic  $\text{In}_2\text{O}_3:(\text{Mn}, \text{Co})$ , which support our previous report that the coexistence of  $\text{Mn}^{2+}$  and  $\text{Mn}^{3+}$  is mandatory for room-temperature ferromagnetism in  $\text{In}_2\text{O}_3:(\text{Mn}, \text{Fe})$  [6], while coexistence of  $\text{Mn}^{2+}$  and  $\text{Mn}^{3+}$  is also found in paramagnetic  $\text{In}_2\text{O}_3:(\text{Mn}, \text{Cr})$ . It should be noted here that the ratios between  $\text{Mn}^{2+}$  and  $\text{Mn}^{3+}$  are different in  $\text{In}_2\text{O}_3:(\text{Mn}, \text{Cr})$  and  $\text{In}_2\text{O}_3:(\text{Mn}, \text{Fe})$ , which suggests that the ratio between  $\text{Mn}^{2+}$  and  $\text{Mn}^{3+}$  is also quite important for the appearance of room-temperature ferromagnetism.

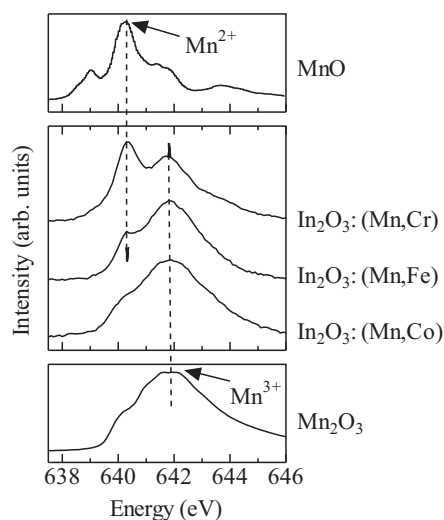


Fig. 1. Observed Mn-L<sub>3</sub> XANES spectra of  $\text{In}_2\text{O}_3:(\text{Mn}, \text{TM})$  (TM=Cr, Fe, Co). Top and bottom spectra are those of MnO [7] and  $\text{Mn}_2\text{O}_3$ , respectively.

- [1] H. Ohno *et al.*, Phys. Rev. Lett. **68** (1992) 2664.
- [2] T. Dietl *et al.*, Science **287** (2000) 1019.
- [3] P. Sharma *et al.*, Nat. Mater. **2** (2003) 673.
- [4] G. Peleckis *et al.*, Appl. Phys. Lett. **88** (2006) 132507.
- [5] T. Yamamoto *et al.*, J. Phys. : Condens. Matter **21** (2009) 104211.
- [6] T. Okazaki *et al.*, Solid State Comm. **151** (2011) 1749.
- [7] B. Gilbert *et al.*, J. Phys. Chem. A **107** (2003) 2839.

## Angle-Resolved Photoemission Study of $\text{CaCu}_3\text{Ti}_4\text{O}_{12}$

H. J. Im<sup>1</sup>, M. Tsunekawa<sup>2</sup>, T. Sakurada<sup>1</sup>, M. Iwataki<sup>1</sup>, K. Kawata<sup>1</sup>, T. Watanabe<sup>1</sup>,  
K. Takegahara<sup>1</sup>, H. Miyazaki<sup>3</sup>, M. Matsunami<sup>4,5</sup>, T. Hajiri<sup>4,6</sup> and S. Kimura<sup>4,5</sup>

<sup>1</sup>Department of Advanced Physics, Hirosaki University, Hirosaki 036-8224, Japan

<sup>2</sup>Faculty of Education, Shiga University, Shiga 522-8522, Japan

<sup>3</sup>Department of Environmental and Materials Engineering, Nagoya Institute of Technology, Nagoya 466-8555, Japan

<sup>4</sup>UVSOR Facility, Institute for Molecular Science, Okazaki 444-8585, Japan.

<sup>5</sup>School of Physical Sciences, The Graduate University for Advanced Studies, Okazaki 444-8585, Japan.

<sup>6</sup>Graduate School of Engineering, Nagoya University, Nagoya 464-8603, Japan

A-site ordered perovskite  $\text{CaCu}_3\text{Ti}_4\text{O}_{12}$  has been attracted much attention due to the extremely high dielectric constant and Mott-type insulator, respectively [1]. However, there have been difficulties to realize applications and understand the underlying physics, e.g. strong correlation effects, due to the absence of experimental band structures. Therefore, we have been studied the electronic structure by the photoemission spectroscopy [2, 3]. In this report, we present the band dispersions obtained the angle-resolved photoemission (ARPES) measurements and discuss the strong correlation effects by comparing with the band calculations within the local-density approximation (LDA).

ARPES experiments were performed at the beamline BL5U. The used photon energy and the total energy resolution are 90 eV and 165 meV, respectively. Measurement temperature is about 300 K. The clean surface was prepared in the (100) plane by cleaving *in situ* in a vacuum better than  $2 \times 10^{-8}$  Pa.

Figure 1 (a) and (b) are the image of the ARPES spectra obtained by the second derivatives of the energy distribution curves and the band dispersions obtained from the LDA calculations, respectively. In Fig. 1 (a), the calculated band dispersions are superimposed on the ARPES image, shifting to the higher binding energy by 1.7 eV. Before comparing the ARPES results and the LDA calculations, it should be noted that there are 51 bands in the valence band region as shown in Fig. 1 (b). Unfortunately, the ARPES experiments cannot resolve these bands due to the limitation of energy- and momentum-resolution. Therefore, the band dispersions observed in ARPES experiments should be interpreted as a bundle of bands with the similar tendency.

In the region of 0 - 2.5 eV, we find the flat band with weak intensity. Even though the exact size of band dispersion cannot be estimated in the ARPES measurements due to the band broadening, we find that the band width is very narrow compared with the LDA calculations. This indicates that the bands are more localized than the expectation of the LDA calculations. These bands are assigned to three bands from 64 to 66 which cross the Fermi level and

disperse by about 1 eV in the LDA calculations. In the region of 2.5 - 5 eV, there are bands around 3 eV and bands around 3.8 eV, which are well consistent with the LDA calculations. The former and the latter bands are assigned to bands from 60 to 63 and from 55 to 59, respectively. Particularly, the bands around 3.8 are not dispersive and show the localized character.

In the region of 5 - 8 eV, ARPES data show the highly dispersive bands, which consist of many bands from 16 to 50 in the LDA calculations.

As discussed above, we attribute the differences between ARPES results and the LDA calculations to the strong correlation effects.

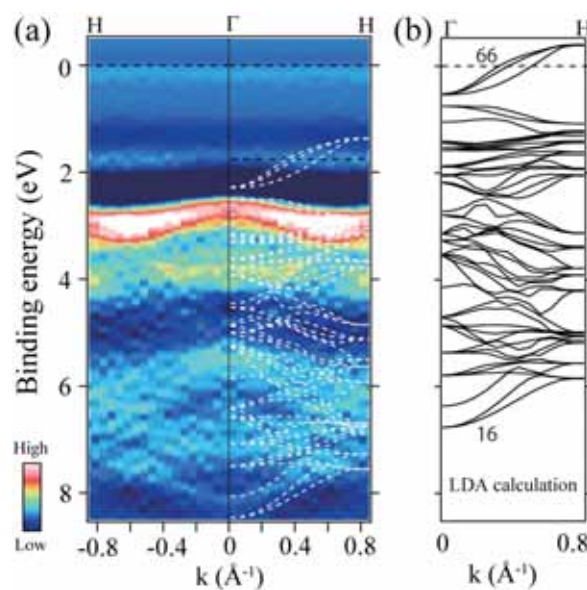


Fig. 1. (a) ARPES image of  $\text{CaCu}_3\text{Ti}_4\text{O}_{12}$  obtained at  $h\nu = 90$  eV and  $T = 300$  K and the band dispersions obtained from the LDA calculations.

[1] M. A. Subramanian *et al.*, J. Solid State Chem. **151** (2000) 323.

[2] H. J. Im *et al.*, UVSOR Activity Report **38** (2011) 87.

[3] H. J. Im *et al.*, UVSOR Activity Report **39** (2012) 90.

## Photoemission Study of Pyrite-type $\text{Ni}_{1-x}\text{Cu}_x\text{S}_2$

K. Soda<sup>1,2,3</sup>, K. Usui<sup>2</sup>, S. Osawa<sup>3</sup>, H. Kondo<sup>1</sup>, M. Kato<sup>1,2,3</sup>, J. Iwasaki<sup>4</sup>, K. Niwa<sup>2,3,4</sup>,  
K. Kusaba<sup>2,3,4</sup> and M. Hasegawa<sup>2,3,4</sup>

<sup>1</sup>Department of Quantum Engineering, Graduate School of Engineering, Nagoya University,  
Nagoya 464-8603, Japan

<sup>2</sup>Department of Physical Science and Engineering, School of Engineering, Nagoya University,  
Nagoya 464-8603, Japan

<sup>3</sup>Department of Materials, Physics and Energy Engineering, Graduate School of Engineering,  
Nagoya University, Nagoya 464-8603, Japan

<sup>4</sup>Department of Crystalline Materials Science, Graduate School of Engineering, Nagoya University,  
Nagoya 464-8603, Japan

Pyrite-type transition-metal dichalcogenides  $\text{MX}_2$  ( $M = \text{Fe}, \text{Co}, \text{Ni}, \text{Cu}, \text{Zn}$ ;  $X = \text{S}, \text{Se}$ ) show rich variety of electronic and magnetic properties due to the electron correlation and hybridization effects.  $\text{NiS}_2$  is classified as a charge-transfer-type insulator and  $\text{NiS}_{2-x}\text{Se}_x$  reveals a metal-insulator transition [1, 2].  $\text{CuS}_2$  is a p-band metal, exhibiting superconductivity [3]. It is interesting to clarify the effects of solid solution between metallic  $\text{CuS}_2$  and insulating  $\text{NiS}_2$  on the electronic structure and related properties. Here, we will report the first preliminary results.

Photoelectron measurements were performed at 10 K at BL5U in angle-integrated mode. Polycrystalline specimens of  $\text{Ni}_x\text{Cu}_{1-x}\text{S}_2$  were synthesized under a high pressure of 6.5 GPa at a temperature of  $\sim 920$  K. Their clean surfaces for the measurement were prepared by scraping them with a diamond file. Total energy resolution was estimated as  $\sim 0.07$  eV at the excitation photon energy of 40 eV. The origin of the binding energy  $E_B$  was set to the Fermi energy  $E_F$  determined by measuring the Fermi edge of an evaporated Au film electrically connected to the specimen.

In Fig. 1, typical valence-band photoelectron spectra of  $\text{Ni}_x\text{Cu}_{1-x}\text{S}_2$  are compared with their X-ray ones obtained at SPring-8 (dots) and calculated results: configuration-interaction cluster model (bars) [4] and band structure (curves) [1, 5] calculations. Each spectrum is normalized with the intensity integrated up to  $E_B = 16$  eV and the excitation photon energy is indicated in the figure. Calculated semiconductor-like electronic structure of  $\text{NiS}_2$  is presented so as to locate the valence-band maximum at  $E_F$ . For  $\text{CuS}_2$ , the observed valence-band spectrum agrees well with the calculated band structure [5], while the present  $\text{NiS}_2$  spectra are in less agreement but consistent with both the calculated results [1, 4]. The intensity at  $E_F$  for  $\text{CuS}_2$  is 50 % of the edge jump, indicating its metallic nature, while that for  $\text{NiS}_2$  is  $\sim 20$  %, suggesting that  $\text{NiS}_2$  has a semimetallic or semiconducting (insulating) feature, as reported [2, 3]. Bands at 2.0 and 2.6 eV in  $\text{NiS}_2$  and  $\text{CuS}_2$  are ascribed to the Ni and Cu 3d states, respectively. In  $\text{Ni}_{0.5}\text{Cu}_{0.5}\text{S}_2$ , peaks are recognized at  $E_B = 1.7$  and 2.6 eV, and the intensity at  $E_F$  is  $\sim 40$  % of the edge jump,

which is in the middle of  $\text{NiS}_2$  and  $\text{CuS}_2$ . Thus the valence band of  $\text{Ni}_{0.5}\text{Cu}_{0.5}\text{S}_2$  seems superposition of those of  $\text{NiS}_2$  and  $\text{CuS}_2$ , although the Ni 3d peak in  $\text{Ni}_{0.5}\text{Cu}_{0.5}\text{S}_2$  is 0.3 eV lower in  $E_B$  than in  $\text{NiS}_2$ , which suggests the hybridization between Ni and Cu states.

Further study is intended on the  $x$ -dependence of the spectral shape as well as the electric and magnetic properties. In comparison to the reported results [1-4], some modifications are also found in the high binding energy region. Further examination will be tried in different experimental conditions including sample preparation.

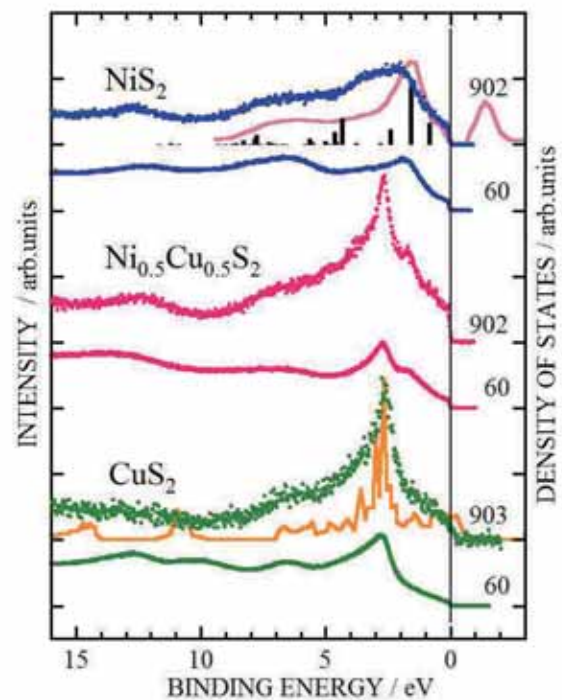


Fig. 1. Valence-band spectra of  $\text{Ni}_{1-x}\text{Cu}_x\text{S}_2$ .

- [1] J. Kunes *et al.*, Phys. Rev. B **81** (2010) 035122.
- [2] K. Mamiya *et al.*, Phys. Rev. B **58** (1998) 9611.
- [3] H. Ueda *et al.*, Phys. Rev. B **65** (2002) 155104.
- [4] A. Fujimori *et al.*, Phys. Rev. B **54** (1996) 16329.
- [5] D. W. Bullett, J. Phys. C **15** (1982) 6163.

## Angle-Resolved Photoemission Study on $\text{Sm}_{1-x}\text{Y}_x\text{S}$

M. Kaneko<sup>1,2</sup>, M. Saito<sup>3</sup>, T. Ito<sup>1,5</sup>, K. Imura<sup>4</sup>, T. Hajiri<sup>1,2</sup>, M. Matsunami<sup>2,6</sup>, S. Kimura<sup>2,6</sup>,  
H. S. Suzuki<sup>7</sup> and N. K. Sato<sup>4</sup>

<sup>1</sup> Graduate School of Engineering, Nagoya University, Nagoya 464-8603, Japan

<sup>2</sup> UVSOR Facility, Institute for Molecular Science, Okazaki 444-8585, Japan

<sup>3</sup> School of Physical Sciences, Nagoya University, Nagoya 464-8603, Japan

<sup>4</sup> Graduate School of Physical Sciences, Nagoya University, Nagoya 464-8603, Japan

<sup>5</sup> Nagoya University Synchrotron Radiation Research Center, Nagoya University, Nagoya 464-8603, Japan

<sup>6</sup> School of Physical Sciences, The Graduate University for Advanced Studies (SOKENDAI), Okazaki 444-8585, Japan

<sup>7</sup> National Institute for Materials Science, Tsukuba 305-0047, Japan

Samarium monosulfide ( $\text{SmS}$ ) is a prototypical valence fluctuating compound inducing insulator (Black phase) – metal (Golden phase) transition by applying external pressure. To directly observe the pressure-induced change of the electronic structure, we have performed angle-resolved photoemission spectroscopy (ARPES) on  $\text{Sm}_{1-x}\text{Y}_x\text{S}$  where the analogous insulator – metal transition is achieved as a function of chemical pressure (Sm-Y substitution).

Single crystals of  $\text{Sm}_{1-x}\text{Y}_x\text{S}$  ( $x = 0, 0.17, 0.33$ ) were grown by the Bridgman technique using a high-frequency induction furnace installed at NIMS. ARPES measurement on these crystals was performed at the VUV-ARPES beamline BL5U of UVSOR-III. The inner potentials  $V_0$  have been 0.17, and 0.33, respectively, by analyzing  $h\nu$ -dependence (27 - 84 eV) of energy distribution curve of highly-dispersive S 3p bands.

Figure 1 (a), (b) and (c) show the ARPES image of  $\text{Sm}_{1-x}\text{Y}_x\text{S}$  ( $x = 0, 0.17$  and  $0.33$ ) near the X point. From the comparison with the reported ARPES on black  $\text{SmS}$  [1], the highly dispersive features at 3 – 6 eV are ascribed to S 3p band, while nondispersive structures, respectively. By Sm-Y substitution, the latter structure gradually shifts to EF, while the former to higher binding energies from  $x = 0.17$  to 0.33 (see Fig.1 (d)).

To investigate the electronic structure, we show the ARPES image of  $\text{Sm}_{0.83}\text{Y}_{0.17}\text{S}$  near EF around the X point at the Brillouin zone boundary [Fig. 1(e)]. We clearly found EF crossing of highly dispersive band around the X point, where the Sm 5d states locate just above EF on black  $\text{SmS}$  [2]. Around the bottom of the dispersive band, the Sm 4f state pushed up to around 0.5 eV show sizable dispersion. The observed Sm 4f dispersion strongly suggests the existence of the Sm 4f-5d hybridization, which causes the insulator to metal transition with Sm-Y substitution.

In conclusion, as the  $\text{Sm}^{2+}$  4f multiplet structure shifts to EF from  $x = 0$  to 0.17, the electron pocket appears due to the Sm 4f-5d hybridization band formation, which is the possible origin of insulator-metal transition. On the other hand, the S 3p bands pushed down to high binding energy side from  $x = 0.17$  to 0.33 since the Sm 5d – S 3p hybridization becomes stronger in the metallic phase.

[1] T. Ito, A. Chainani, H. Kumigashira, T. Takahashi and N. K. Sato, Phys. Rev. B **65** (2002) 155202.

[2] V. N. Antonov *et al.*, Condensed Matter Physics, **7** (2004) 38.

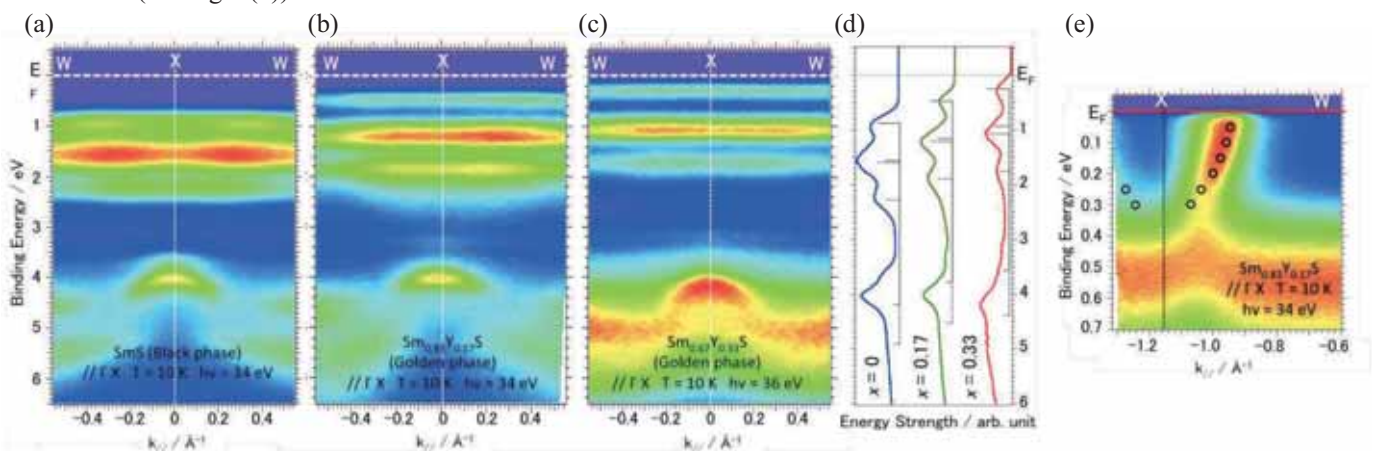


Fig. 1. The ARPES image of (a)  $x = 0$ , (b) 0.17 and (c) 0.33 near the X point.

(d) The elemental substitution dependence of the ARPES spectrum at X point ( $x = 0, 0.17$  and  $0.33$ )

(e) The thorough ARPES image of  $x = 0.17$ . Open circles indicate the peak positions of the bands estimated by the second derivative of EDC data.

# Annealing Behavior of Ultrashallow Thermal Donors Formed in Carbon- and Hydrogen-Doped Czochralski Silicon Crystals

A. Hara and T. Awano

*Electronic Engineering, Tohoku Gakuin University, Tagajo 985-8537, Japan*

In the past, we have reported on ultrashallow thermal donors (USTDs) in carbon- and hydrogen-doped Czochralski silicon (CZ Si) crystals after annealing at 480°C [1]. USTDs are hydrogen-like donors with slightly different energy levels, some of which show negative central-cell correction, and to the best of our knowledge, are the shallowest energy levels as compared to many types of previously reported donors in Si crystals [2]. In this study, we evaluated the relationship between the intensity of USTDs and annealing time to investigate their formation mechanism.

Carbon-doped CZ Si samples were doped with hydrogen by annealing them in wet oxygen at 1300°C for 60 min. The samples were then cooled to room temperature by rapidly exposing them to air. For carbon doping, the Si melt used for preparing the ingot was doped with carbon powder during CZ Si crystal growth. The formation of USTDs at 480°C in wet oxygen was investigated using the far-IR spectrometer of the BL6B beamline at Liq. He temperature obtained using a flowing cryostat.

Figure 1 shows the annealing behavior of USTDs and shallow thermal donors (STDs). It has been reported that STDs are hydrogen-like donors and are generated in hydrogen-doped CZ Si crystals at around 450°C [3]. STDs are generated rapidly within the first 10 h and then decrease with the annealing time. However, USTDs are generated slowly and increase with increasing annealing time.

Figure 2 shows that the intensity of STDs after annealing at 480°C for 40 h is equal to that after 10 h of annealing in hydrogen-doped but without carbon CZ Si crystals. Moreover, USTDs are not generated.

Figures 1 and 2 show that carbon impurities act as atomic elements essential for the generation of USTDs and reduction of STDs. Carbon impurities occupy substitution sites; therefore, its diffusion coefficient ( $D$ ) is very small given by  $D = 1.9\exp(-3.2\text{eV}/k_{\text{B}}T) \text{ cm}^2/\text{s}$  [4]. However, the value of  $D$  for interstitial carbons is significantly greater than this value. Thus one tentative explanation for the results shown in Figure 1 and 2. They are that some STDs, which are generated in the initial stage at 480°C owing to their rapid generation rate, are transformed to USTDs during long-term annealing by combining with interstitial carbons. Interstitial carbon is thought to be generated in CZ Si by the formation of  $\text{SiO}_2$  precipitates.

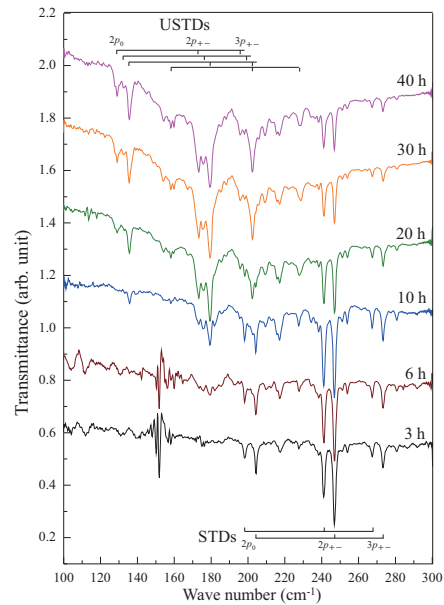


Fig. 1. Variations in USTDs and STDs after annealing at 480°C in carbon- and hydrogen-doped CZ Si crystals.

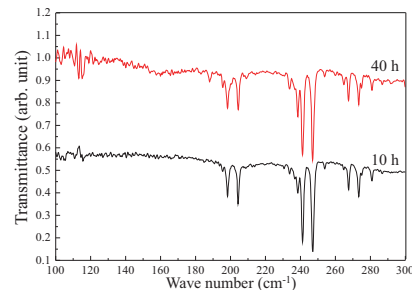


Fig. 2. Spectra for STDs after annealing at 480°C for 10 and 40 h in hydrogen-doped but without carbon CZ Si crystals.

- [1] A. Hara, T. Awano, Y. Ohno and I. Yonenaga, *Jpn. J. Appl. Phys.* **49** (2010) 050203.
- [2] A. Hara, *Jpn. J. Appl. Phys.* **34** (1995) 3418.
- [3] R. C. Newman, J. H. Tucker, N. G. Semaltianos, E. C. Lightowers, T. Gregorkiewicz, I. S. Zevenbergen and C. A. J. Ammerlaan, *Phys. Rev. B* **54** (1996) R6803.
- [4] F. Shimura, *Semiconductor Silicon Crystal Technology* (Academic Press, 1988)

## Study of Electronic States of Solids Probed by a Microspectroscopy Using the Synchrotron Radiation

A. Irizawa<sup>1</sup>, S. Kobayashi<sup>2</sup>, K. Yoshimura<sup>2</sup> and S. Kimura<sup>3,4</sup>

<sup>1</sup>The Institute of Science and Industrial Research, Osaka University, Ibaraki 567-0047, Japan

<sup>2</sup>Division of Chemistry, Graduate School of Science, Kyoto University, Kyoto 606-8502, Japan

<sup>3</sup>School of Physical Sciences, The Graduate University for Advanced Studies (SOKENDAI), Okazaki 444-8585, Japan

<sup>4</sup>UVSOR Facility, Institute for Molecular Science, Okazaki 444-8585, Japan

The optical study using infrared light sources is one of the most powerful techniques for the investigation of electronic states on solids. There can be obtained the direct information about the change of electronic band structure, the symmetry of crystal structure, and the dielectric property. In the respect of experimental affinity, the optical study is extremely compatible with the multiple conditions such as low temperature, high magnetic field, and high pressure. In the case of strongly correlated electron systems, it is well known that the temperature is one of the decisive factors for the electronic state. The considerable types of phase transition are induced by the change of the temperature. Particularly, the multiferroic compounds can be controlled of its physical properties mutually by the external fields such as magnetic, electronic, and elastic ones. The other particular condition, the pressure will directly affect the electron-electron interactions through the change of lattice constants. The beamline 6B in UVSOR is adjusted for the investigations at low temperature and high pressure in the extremely low-energy region of FIR-THz (far infrared-terahertz). There equips two type interferometers of both Michelson and Martin-Puplett type. In this report, we tried the optical reflectivity measurements in the longest wavelength region by a micro spectrometer for the single crystals of newly synthesized compound CrSe<sub>2</sub> showing a discontinuous resistive change and a pressure-dependent magnetization.

The experiments are performed using a micro spectrometer having 1D array detector and a liquid-He flow type cryostat for controlling the temperature from 300 K down to 20 K. The reflectivity was obtained from the ratio of optical reflections between the sample and Au as a standard with mirrored surfaces. They were installed on the sample holder and were measured through a polypropylene window of the cryostat.

The reflectivities are obtained in the energy range between 200 and 700 cm<sup>-1</sup> as shown in Fig. 1. This compound shows two discontinuous temperature changes at 195 K and at 175 K with hysteresis loop in electrical resistivity [1] and magnetization [1, 2], but from the results of optical reflectivity experiments there is no significant change in the energy range of

FIR. At this moment it comes out that the lower energy experiments using larger samples are demanded as a future study for this compound.

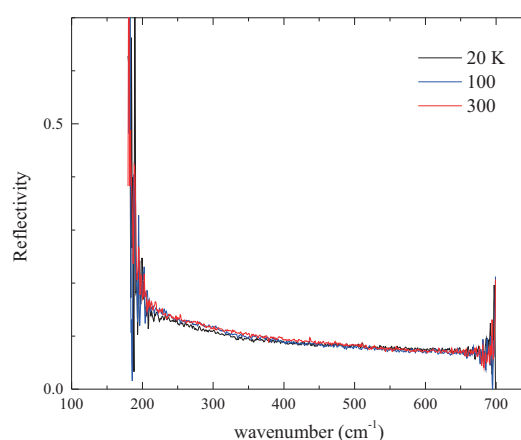


Fig. 1. Temperature change of reflectivity of CrSe<sub>2</sub>.

[1] S. Kobayashi *et al.*, 18pGB-12 (2012) JPS meeting in Yokohama.

[2] C.F. van Bruggen *et al.*, Physica B+C **99** (1980) 166.

## Increase of Quasiparticle Lifetime in FeSb<sub>2</sub> Kondo-Semiconductor

T. Takeuchi<sup>1,2,3</sup>, T. Shimada<sup>3</sup>, M. Matsunami<sup>4</sup> and S. Kimura<sup>4</sup>

<sup>1</sup>EcoTopia Science Institute, Nagoya University, Nagoya 464-8603, Japan

<sup>2</sup>PRESTO, Japanese Science and Technology Agency, Tokyo 102-0075, Japan

<sup>3</sup>Department of Applied Physics Graduate School of Engineering, Nagoya University, Nagoya 464-8603, Japan

<sup>4</sup>UVSOR, Institute for Molecular Science, Okazaki 444-8585, Japan

FeSb<sub>2</sub> has attracted interest because it possesses a huge magnitude of Seebeck coefficient  $|S|$  exceeding 40 mV/K at low temperature below 40 K [1]. The origin of this huge  $|S|$  has not been revealed yet. Seebeck coefficient is generally determined by the electronic structure near the chemical potential of conduction electrons. Thus it is of great importance to investigate its electronic structure in detail. Since the unusual increase of  $|S|$  is observed at low temperatures below 50 K, one has to use experiments that are capable of investigating the detailed electronic structure with a high-energy resolution.

In this study, therefore, we prepared high-quality single grained FeSb<sub>2</sub> samples and measured their electronic structure in detail by means of high-resolution angle resolved photoemission spectroscopy measurements (ARPES) with synchrotron radiation as the photon source at BL7U of UVSOR. We also measured Seebeck coefficient, low temperature specific heat, and magnetization over a wide temperature range from 2 K to 100 K.

The single grained FeSb<sub>2</sub> samples were grown in antimony flux under the vacuum atmosphere. The electrical resistivity shows a very large but finite value at low temperature. This result indicates a finite number of electronic states persisting at the Fermi energy ( $\varepsilon_F$ ). We also confirmed that the electronic specific heat coefficient of samples was distributed

over the range of  $0.001 < \gamma < 0.01 \text{ mJ mol}^{-1}\text{K}^{-2}$ . These small  $\gamma$  definitely indicate the very small but finite value of electronic density of states at  $\varepsilon_F$ .

We also realized that the shape of ARPES spectra drastically changes with varying temperature. The sharp peak persisting at temperatures below 20 K starts to be broadened above 30 K. The drastic increase of the energy-width of spectral function indicates that the quasiparticle lifetime is fairly reduced. Notably, this temperature dependence was observed over the whole momentum-range where the present ARPES measurement was performed.

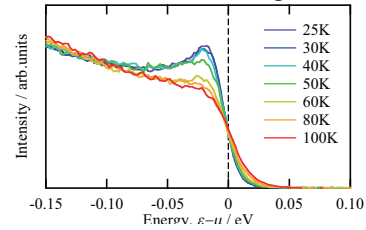


Fig. 2. Energy distribution curves observed at a momentum near the Fermi surface. With decreasing temperature, the peak intensity drastically increased at the temperature range below 60 K where the large magnitude of Seebeck coefficient was observed.

At the same temperature range, the magnitude of Seebeck coefficient and electrical resistivity decreases with increasing temperature, while the magnitude of magnetic susceptibility increases. All the experimental facts unambiguously indicate that the electronic structure change in association with destruction of Kondo-lattice occurs with increasing temperature in this particular temperature range. If we assume the formation of Kondo-peak a few meV above the chemical potential at the temperature range below 30 K, the large magnitude of Seebeck coefficient with negative sign is reasonably accounted for with it. The behavior of electrical resistivity above 30 K is understood as that in the disordered Kondo materials where the lifetime of quasiparticle is limited to be short by the strong spin scatterings. The constant value of electrical resistivity below 30 K is regarded as that observed for Kondo lattice under the unitary limit in good consistency with the rather long lifetime of quasiparticles. The increase of magnetic susceptibility with increasing temperature above 30 K is also accounted for with the destruction of Kondo lattice leading to the development of local magnetic moment.

[1] T. Bienten *et al.*, EPL **80** (2006) 17008.

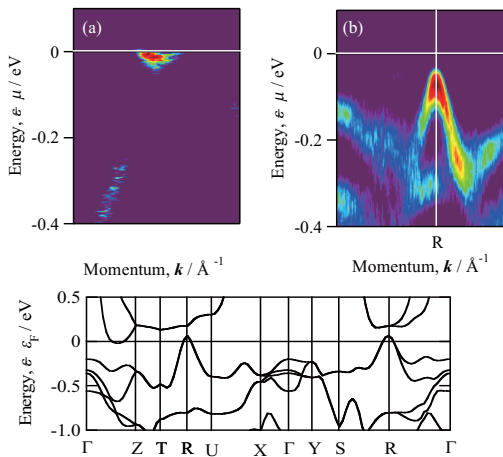


Fig. 1. (a) Electron pocket observed in the second momentum derivative of ARPES intensity  $\partial I(k_{TZ}, \varepsilon)/\partial k_{TZ}$  measured along  $\Gamma$ -Z line. (b) Second energy derivative of ARPES intensity  $\partial I(k_{TR}, \varepsilon)/\partial \varepsilon$  obtained at a momentum line near R. The band dispersion calculated by FLAPW-GGA is shown in the bottom.

# Investigation of the Electron-phonon Scattering in the Graphite by Using the Angle-Resolved Photoelectron Spectroscopy: Direct Observation of the Indirect Transition

S. Tanaka<sup>1</sup>, M. Matsunami<sup>2,3</sup> and S. Kimura<sup>2,3</sup>

<sup>1</sup>The Institute of Scientific and Industrial Research, Osaka University, Ibaraki 567-0047, Osaka, Japan

<sup>2</sup>UVSOR Facility, Institute for Molecular Science, Okazaki 444-8585, Japan

<sup>3</sup>School of Physical Sciences, The Graduate University for Advanced Studies (SOKENDAI), Okazaki 444-8585, Japan

The electron-phonon scattering is one of the key issues in the solid state physics and has been extensively studied for long years. Angle-resolved photoelectron spectroscopy (ARPES) is a very powerful tool to investigate the electronic properties of the condensed matter, since it allows us to measure the band of the electron resolving both in energy and momentum. Then, it has been used to understand the electron-phonon scattering in solids by many researchers. With the ARPES spectrum, however, the electron-phonon interaction was investigated only through the self-energy of the quasiparticle-spectral function in an integrated manner over their branches and momentum. In this study, our aim is observing directly the process of electron-phonon scattering with resolving the energy and momentum. If the energy and momentum of the electron before the scattering are known, the measurements for those of the scattered electron allow us to determine the energy and momentum of the phonons that scattered the electron thanks to the law of the conservation.

For this purpose, we took the Graphite as a target material. HOPG (highly oriented pyrolytic graphite) sample was cleaved *in-situ* and investigated with the ARPES at BL7U of the UVSOR-III. The sample temperature was kept at 50K, that is higher than the critical temperature for the CDW transition [1]. Figure 1(a) shows the surface-normal photoelectron spectra taken at photon energies from 6 to 16eV. The spectra vary drastically depending on the photon energy, and Fig. 1(b) shows the typical spectra in detail. The step-like edges are clearly observed not at the Fermi level, where an edge is observed for the Au film, but at 68meV and 155meV with respect to the Fermi level. Differentials of the spectra are shown in Fig. 1(c) for a convenience to eye, and the peaks are clearly observed at the edge positions. The electronic band crosses the Fermi level at K(H)-point in the Brillouin zone of Graphite and highest occupied band at the  $\Gamma$ (A)-point is located at  $\sim 4$ eV below the Fermi level. Therefore, the electron emission observed in Fig. 1(a) is due to the electron scattering from the K(H)-point to the  $\Gamma$ (A)-point. When the electron-phonon interaction occurs, the electron loses (emission) or gains (absorption) its energy as much as the phonon energy. Since temperature is low (50K), the phonon-absorption probability is negligible in this case. Thus, the peak positions should indicate the

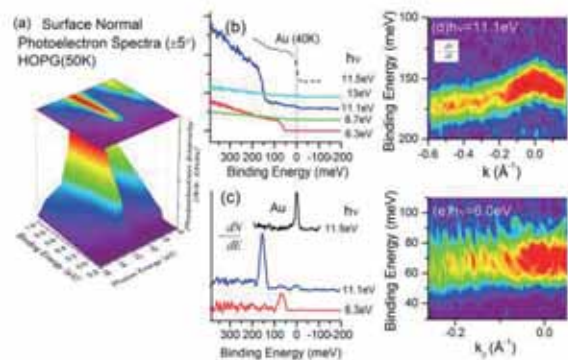


Fig. 1. ARPES Spectra for Graphite (HOPG) and their differentials with respect to the binding energy of the electrons.

energies of the phonons that scattered the electron. Moreover, considering the conservation rule for the momentum, the angle-resolved measurement of the photoelectron enables us to investigate the dispersions of the phonons around the K(H)-point. The angle-resolved differential spectra are shown in Figs. 1(d) and (e) taken at  $h\nu=11.1$ eV and 6.0eV, respectively. They clearly show the dispersions of the phonons.

68meV and 155meV phonons are attributed to the ZA and/or ZO, and LO and/or LA modes, respectively. The strong photon-energy-dependence observed in Fig. 1(a) indicates that the final state of the photoexcitation determines the phonon branch that can scatter the electron during the photoexcitation process. It should be ascribed to the dipole selection rules both for the optical transition and the electron-phonon scattering, those of which can be predicted by using the group theory. The detail will soon be published elsewhere.

[1] S. Tanaka, M. Matsunami and S. Kimura, Phys. Rev. B **84** (2011) 121411(R).

## Change in the Electronic Structure of the Single Crystalline Graphite as a Result of the CDW Transition

S. Tanaka<sup>1</sup>, M. Matsumoto<sup>2</sup>, M. Matsunami<sup>3,4</sup> and S. Kimura<sup>3,4</sup>

<sup>1</sup>The Institute of Scientific and Industrial Research, Osaka University, Ibaraki 567-0047, Osaka, Japan

<sup>2</sup>Institute of Industrial Science, The University of Tokyo, 4-6-1 Komaba, Meguro-ku, Tokyo 153-8505, Japan.

<sup>3</sup>UVSOR Facility, Institute for Molecular Science, Okazaki 444-8585, Japan

<sup>4</sup>School of Physical Sciences, The Graduate University for Advanced Studies (SOKENDAI), Okazaki 444-8585, Japan

Charge-density-wave (CDW) transition is one of the topics that have been extensively studied in solid state physics. This phenomenon is a rearrangement of the atomic structure of low-dimensional solids due to the electron-photon interaction. When the temperature is below critical temperature for the CDW transition, the superstructure is formed accompanying the opening of the gap near the Fermi level in the electronic structure. Recently, we found the experimental evidence that the  $p(\sqrt{3} \times \sqrt{3})R30^\circ$  superstructure is formed at lower temperature than 30K on the HOPG (Highly Oriented Pyrolytic Graphite) with Angle-resolved photoelectron spectroscopy (ARPES), and interpreted it as the CDW transition according to the temperature-dependent measurement [1]. When the superstructure is formed, the folding of the Brillouin zone occurs, and the dispersion (originally) at the K-point can be observed at the  $\Gamma$ -point with the ARPES. However, a change in the electronic states as a result of the CDW transition was not observed in the previous work. This is somewhat paradoxical. In this paper, therefore, we examine a change in the electronic structure due to the CDW transition on the single-crystal of Graphite.

The experiments were carried out at BL-7U. The single-crystalline Graphite samples exhibited sharp (1x1) LEED (Low Energy Electron Diffraction) pattern. A clean surface was made by cleaving using the Scotch tape in the ultrahigh vacuum at low temperature. The superstructure formed at low temperature below 30K was confirmed using the 11.5eV-photons in the same manner as the previous study [1]. The photon energy used below was 39eV.

The left panel of Fig.1 shows the comparison of the ARPES spectra near the K-point along the  $\Gamma$ -K-M' direction when the sample temperature is changed from 15K to 50K, those are respectively below and above the critical temperature of the CDW transition. No significant differences are observed in the main features, which show the dispersion of the  $\pi$ -band of the Graphite as previously reported. However, there is a striking change for a dispersive band indicated by circles in the left panel of Fig.1. For showing more detail, we display the EDC curves at several  $k_{||}$  values in the right panel of Fig. 1. At top curves, where the  $\pi$

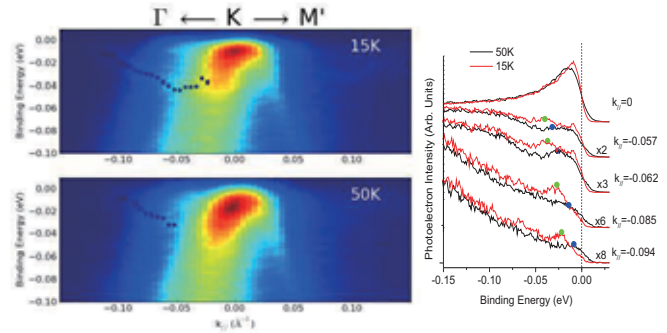


Fig. 1. ARPES Spectra near the K-point of the single-crystalline Graphite at 15K and 50K.

band at the K-point is only observed, there is no change except the thermal broadening at 50K. Meanwhile, the spectrum at higher  $k_{||}$  show changes with changing temperature. The energy positions of the green (15K) and blue (50K) circles correspond to those of the circles in the left panel of Fig. 1. This band shifts in energy to by about 0.01eV when the temperature is changed. At 50K, this band crosses the Fermi level at  $k_{||} \sim 0.1\text{\AA}^{-1}$  while the gap seems open at 15K where the CDW is formed.

According to the report by Zhou et al. [2], this band is ascribed to the edge state of the zig-zag step on the Graphite surface. Sugawara et al. also reported a similar band [3]. Therefore, we can conclude that the CDW transition is strongly related to the edge state. The band folding at low temperature may be ascribed to the surface Umklapp process that is due to the CDW transition at domains near to the step edge on the Graphite surface. This is consistent with the theoretical calculation by Hamada et al. [4].

- [1] S. Tanaka M. Matsunami and S. Kimura, Phys. Rev. B **84** (2011) 121411(R).
- [2] S.Y. Zhou, G.-H. Gweon and A. Lanzara, Ann. of Phys. **321** (2006) 1730–1746.
- [3] K. Sugawara, T. Sato, S. Souma, T. Takahashi and H. Suematsu, Phys. Rev. B. **73** (2006) 045124.
- [4] I. Hamada and Y. Morikawa, Phys. Rev. B **85** (2012) 237401.

## Angle-Resolved Photoemission Study on FeSb<sub>2</sub>

S. Imada<sup>1</sup>, K. Terashima<sup>1</sup>, H. Eto<sup>1</sup>, K. Sano<sup>1</sup>, K. Tsukamura<sup>1</sup> and H. Nakamura<sup>2</sup>

<sup>1</sup>Faculty of Sci. and Eng., Ritsumeikan Univ., Shiga 525-8577 Japan

<sup>2</sup>Grad. School of Eng., Kyoto Univ., Kyoto 606-8501, Japan

FeSb<sub>2</sub> shows a metal-insulator crossover; it is metallic around room temperature, while it is insulating at low temperatures with an upturn of the resistivity curve at  $\sim 50$  K. A number of experimental reports have indicated the existence of the energy gap at low temperatures [1-3], while the mechanism for the formation of the energy gap has not been settled yet. So far, mainly two scenarios have been proposed, one is that FeSb<sub>2</sub> is a Kondo insulator [2], and the other is that FeSb<sub>2</sub> is a narrow-gap semiconductor [1, 3]. FeSb<sub>2</sub> has an orthorhombic structure with  $a = 5.82$  Å,  $b = 6.51$  Å and  $c = 3.17$  Å at 100 K [2].

In our previous study on FeSb<sub>2</sub> at UVSOR [4], we have measured temperature dependence of the density of states (DOS) near  $E_F$ . As we reduce the temperature, the DOS suppression is observed, but finite intensity in the vicinity of  $E_F$  remains even at 15 K where the resistivity shows insulating behavior. We also find a free-electron like band crossing  $E_F$  at 15 K, indicative of the surface state. Thus it is important to separate the surface contribution from photoemission spectra to discuss bulk property and its mechanism.

We have also performed angle-resolved photoemission (ARPES) on FeSb<sub>2</sub> to reveal the mechanism of the crossover by directly observing the temperature dependence of the energy gap. We have observed dispersive bands but interpretation was left ambiguous due to the small amount of data.

In this study, we have performed normal emission measurement with larger photon energy region than the previous measurement and succeeded in observing a clear dispersion.

A single crystal of FeSb<sub>2</sub> has been synthesized by Sb-flux method. High-resolution ARPES study has been performed at BL-7U in the UVSOR facility. Energy resolution was set at  $\sim 13$  meV. We have obtained a clean surface of the sample by fracturing in an ultrahigh-vacuum of  $\sim 1 \times 10^{-8}$  Pa.

Figure 1 (a) shows the normal emission spectra from the (100) surface of FeSb<sub>2</sub> at 100 K using photon energy ( $h\nu$ ) from 12 to 40 eV, where each  $h\nu$  corresponds to different  $k$  points along  $\Gamma$ -X axis. As in Fig. 1(a), we have observed a number of dispersive bands of FeSb<sub>2</sub>, such as Fe  $3d_{3z^2-r^2}$  band [5] located at binding energy ( $E_B$ ) of  $\sim 0.3$  eV, Fe  $3d_{x^2-y^2}$  band [5] at  $E_B \sim 1$  eV, and so on. By comparing the dispersion with the calculated bands [6], we estimate that in the spectrum taken at  $h\nu \sim 35$  eV, the bottom of the valence band at the  $\Gamma$  point is observed at around  $E_B$

$\sim 6$  eV. Reflection of a band around  $E_B \sim 2.5$  eV at X point is found at around  $h\nu \sim 23$  eV. Between these points, a clear dispersion is found. Further ARPES study, clarifying (i) the bulk Fermi surfaces near the Zone edge and corner [5], (ii) the location of the surface bands, (iii) the temperature dependence of bulk bands, is necessary to elucidate the origin of the metal-insulator crossover in FeSb<sub>2</sub>

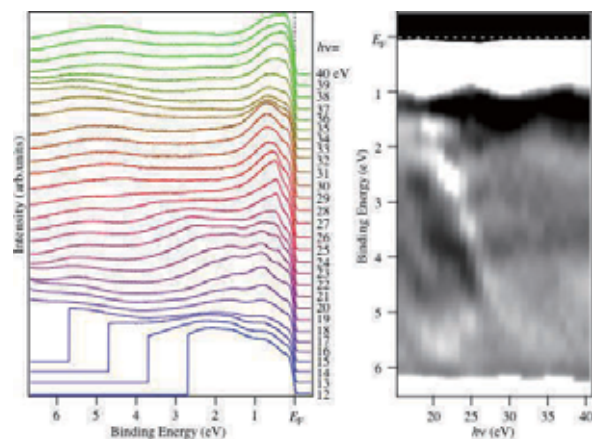


Fig. 1. (a) ARPES spectra derived by normal emission method using  $h\nu = 12$ -40 eV at BL-7U. (b) Plot of second derivative of (a). White area corresponds to bands.

- [1] Z. Schlesinger *et al.*, Phys. Rev. Lett. **71** (1993) 11.
- [2] C. Petrovic *et al.*, Phys. Rev. B **72** (2005) 045103.
- [3] T. Koyama *et al.*, Phys. Rev. B **76** (2007) 073203.
- [4] S. Imada *et al.*, UVSOR Activity Report **37** (2010) 106.
- [5] A. V. Lukoyanov *et al.*, Euro. Phys. J. **53** (2006) 205.
- [6] J. M. Tomczak *et al.*, Phys. Rev. B **82** (2010) 085104.

## Three-Dimensional Electronic Structure of Over-Doped $\text{BaFe}_{1.8}\text{Co}_{0.2}\text{As}_2$

T. Hajiri<sup>1,2</sup>, T. Ito<sup>1,3</sup>, M. Matsunami<sup>2,4</sup>, B. H. Min<sup>5</sup>, Y. S. Kwon<sup>5</sup> and S. Kimura<sup>2,4</sup>

<sup>1</sup>Graduate School of Engineering, Nagoya University, Nagoya 464-8603, Japan

<sup>2</sup>UVSOR Facility, Institute for Molecular Science, Okazaki 444-8585, Japan

<sup>3</sup>Nagoya University Synchrotron radiation Research Center, Nagoya University, Nagoya, 464-8603, Japan

<sup>4</sup>School of Physical Sciences, The Graduate University for Advanced Studies (SOKENDAI), Okazaki 444-8585, Japan

<sup>5</sup>Department of Emerging Materials Science, DGIST, Daegu 711-873, Republic of Korea

In iron pnictides, it is one of the most interest issues that where the nodes appear in three-dimensional (3D) electronic structures. In  $\text{BaFe}_2\text{As}_{2-x}\text{P}_x$  system, there are different two reports. One is that there are the nodes on the hole Fermi surface (FS) of  $d_{z^2}$  orbital character around Z point [1], and the other is that on the electron FS at the longer edge of the ellipsoid-shaped FS cross-section [2]. The former can be explained by spin fluctuation mediated superconductivity theory [3], while the latter by taking into account for not only spin fluctuations but also orbital fluctuations. On the other hand, the fundamental physical properties of  $\text{BaFe}_{2-x}\text{Co}_x\text{As}_2$  system suggest the existence of orbital fluctuations in the wide doping range [4], despite spin fluctuation cannot. Therefore, it is important to determine 3D superconducting gap symmetry.

To elucidate this, we performed a 3D angle-resolved photoemission spectroscopy of over-doped  $\text{BaFe}_{1.8}\text{Co}_{0.2}\text{As}_2$  ( $T_c \sim 22.5$  K) at BL7U, UVSOR-III.

Figure 1(a) shows a 3D hole FSs measured in the  $\Gamma\text{MAZ}$  plane at  $T = 12$  K. The red open circles indicate the hole FSs determined by the peak positions of the momentum distribution curves. One and two hole FSs are clearly visible at  $\Gamma$  and Z point, respectively [Fig. 1(b, c)].

Figure 2(a) shows the symmetrized energy distribution curve (EDC) at  $\Gamma$  point. The symmetrized EDC spectrum at  $T = 35$  K ( $> T_c$ ) shows the pseudogap [5] at around 8 meV. On the other hand, at  $T = 12$  K, the additional shoulder structure appears at around 6 meV. Interestingly, when we divide the symmetrized EDC at  $T = 12$  K by one at  $T = 35$  K, we found that only the low-energy shoulder remains. This suggests that the low-energy shoulder can be identified as superconducting gap, while the high-energy one as ‘pseudogap’. Figure 2(b, c) shows the symmetrized EDC spectra and summarized gap size at several photon energies at 12 K. We can recognize the superconducting gap between 5~7 meV at each photon energy and almost isotropic superconducting gaps. These results imply that there is no horizontal line nodes, at least, on the outer hole FS in this system.

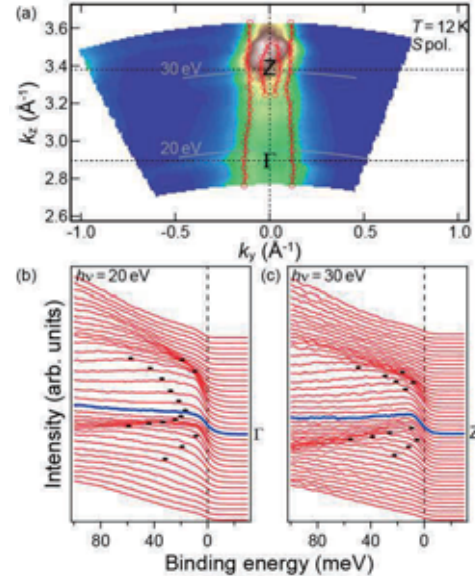


Fig. 1. (a) Out-of-plane FSs in the  $\Gamma\text{MAZ}$  plane at  $T = 12$  K. (b, c) EDC along gray-lines marked by 20 (b) and 30 eV (c) in panel (a), respectively.

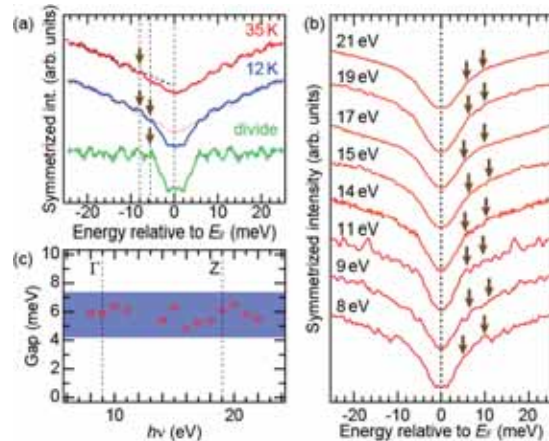


Fig. 2. (a, b) Temperature (a) and photon energy (b) dependent symmetrized EDC. (c) Size of the superconducting gaps estimated from panel (b).

- [1] Y. Zhang *et al.*, Nature Phys. **8** (2012) 371.
- [2] T. Yoshida *et al.*, arXiv:1301. (2013) 4818.
- [3] K. Suzuki *et al.*, J. Phys. Soc. Jpn. **80**, 013710 (2011).
- [4] H. Kontani *et al.*, Solid State Commun. **152** (2012) 718.
- [5] S. Kasahara *et al.*, Nature **486** (2012) 382.

## Angle-Resolved Photoemission Study on Quasi-One-Dimensional Organic Conductor (TMTSF)<sub>2</sub>X (X = SbF<sub>6</sub>, AsF<sub>6</sub>, PF<sub>6</sub>)

M. Mitamura<sup>1</sup>, S. Hirate<sup>2</sup>, T. Hajiri<sup>2</sup>, T. Ito<sup>2,4</sup>, S. Kimura<sup>3,5</sup> and T. Nakamura<sup>3,5</sup>

<sup>1</sup>*School of Engineering, Nagoya University, Nagoya 464-8603, Japan*

<sup>2</sup>*Graduated School of Engineering, Nagoya University, Nagoya 464-8603, Japan*

<sup>3</sup>*UVSOR Facility, Institute for Molecular Science, Okazaki 444-8585, Japan*

<sup>4</sup>*Nagoya University Synchrotron Radiation Research Center, Nagoya University, Nagoya 464-8603, Japan*

<sup>5</sup>*School of Physical Sciences, The Graduate University for Advanced Studies (SOKENDAI), Okazaki 444-8585, Japan*

The Bechgaard salts (TMTSF)<sub>2</sub>X (TMTSF: tetramethyl-tetraselenafulvalene, X = SbF<sub>6</sub>, AsF<sub>6</sub>, PF<sub>6</sub>, etc.) are the well-known models of quasi-one-dimensional (Q1D) organic conductor. At low temperatures, this quasi-one-dimensionality results in an intriguing ground state such as a spin-density-wave (SDW) state, a superconducting state, etc., depending on anion X (or pressure) [1].

In this study, we have performed angle-resolved photoemission spectroscopy (ARPES) on single-crystalline (TMTSF)<sub>2</sub>X (X = SbF<sub>6</sub>, AsF<sub>6</sub>, PF<sub>6</sub>) to clarify the intrinsic electronic structure and its relation to the anomalous properties by utilizing the bulk-sensitive microfocus low-energy photons ( $h\nu = 8$  eV,  $15 \times 150 \mu\text{m}^2$ ).

Figure 1 shows the second derivative of the ARPES image near the Fermi level ( $E_F$ ) along the  $\Gamma X$  high-symmetry line measured at  $T = 30$  K of (TMTSF)<sub>2</sub>X (X = SbF<sub>6</sub>(a), AsF<sub>6</sub>(b), PF<sub>6</sub> (c)), respectively. Three clear band dispersions ( $h$ ,  $s$  and  $p$ ) successfully observed on each compounds. From the comparison with the first principle calculation on analogous (TMTSF)<sub>2</sub>ClO<sub>4</sub>, the hole-like dispersion of main feature ( $\underline{p}$ ) around the  $\Gamma$  point can be assigned as the TMTSF band [2]. Though the theory expects only one TMTSF band, the observed multi dispersive features could be attributed to, so called, spin-charge separation. Actually, the separation of  $\underline{h}$  and  $\underline{p}$  dispersions on (TMTSF)<sub>2</sub>X, respectively, shows good correspondence with holon and spinon bands on inorganic Q1D conductor SrCuO<sub>2</sub> [3].

In the one-dimensional Hubbard model, it is known that, the width of holon and spinon band corresponds to transfer integral along TMTSF chain  $t_a$  (red) and spin-exchange interaction constant  $J$  (blue), respectively. Table 1 shows the comparison of the  $J$  and  $t_a$  estimated by the present ARPES with those by the thermodynamic experiments [4-6]. From the comparison, we found qualitative agreement of  $J$  and  $t_a$  between the experiments. Furthermore, gradual increase of  $t_a / J$  from X = SbF<sub>6</sub> to PF<sub>6</sub> has been revealed, while  $t_a$  shows discontinuity. The results suggests that the balance of bandwidth between holon and spinon should reflect the nature of TMTSF  $\pi$  electrons (localized or itinerant) and scale with the physical properties as well.

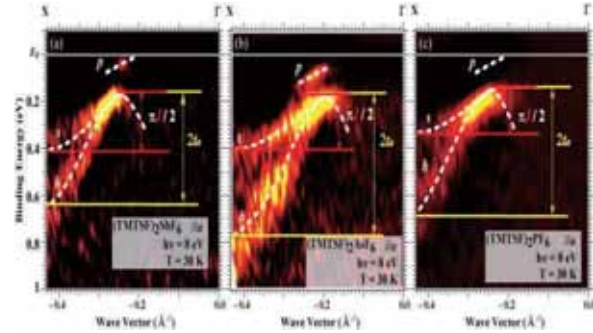


Fig. 1. Second derivative of ARPES image near  $E_F$  of (TMTSF)<sub>2</sub>X (X = SbF<sub>6</sub>(a), AsF<sub>6</sub>(b), PF<sub>6</sub> (c)).

Table 1.  $J$  and  $t_a$  of (TMTSF)<sub>2</sub>X (X = SbF<sub>6</sub>, AsF<sub>6</sub>, PF<sub>6</sub>) estimated by thermodynamic [4-6] and present ARPES experiments.

X=	Thermodynamic		ARPES		
	$J$ (meV)	$t_a$ (meV)	$J$ (meV)	$t_a$ (meV)	$t_a / J$
SbF <sub>6</sub>	—	—	139	212	1.53
AsF <sub>6</sub>	120[4]	250[5]	135	276	2.04
PF <sub>6</sub>	120[4]	230[6] -250[5]	83	200	2.41

[1] T. Ishiguro *et al.*, *Organic Superconductors* (Springer-Verlag, Berlin, 1998).

[2] S. Ishibashi, *Sci. Technol. Adv. Mater.* **10** (2009) 024311.

[3] B. J. Kim *et al.*, *Nat. Phys.* **2** (2006) 397.

[4] M. Dumm *et al.*, *Phys. Rev. B* **62** (2000) 6512.

[5] C. S. Jacobsen *et al.*, *Phys. Rev. B* **28** (1983) 7019.

[6] L. Ducasse *et al.*, *J. Phys. C* **19** (1986) 3805.

## Hybridized Band Dispersion of YbAl<sub>2</sub>

M. Matsunami<sup>1,2</sup>, T. Hajiri<sup>1</sup>, H. Miyazaki<sup>3</sup>, M. Kosaka<sup>4</sup> and S. Kimura<sup>1,2</sup>

<sup>1</sup>UVSOR Facility, Institute for Molecular Science, Okazaki 444-8585, Japan

<sup>2</sup>School of Physical Sciences, The Graduate University for Advanced Studies (SOKENDAI), Okazaki 444-8585, Japan

<sup>3</sup>Center for Fostering Young and Innovative Researchers, Nagoya Institute of Technology, Nagoya 466-8555, Japan

<sup>4</sup>Graduate School of Science and Engineering, Saitama University, Saitama 338-8570, Japan

The most important concept in the heavy fermion systems is a hybridization effect between conduction (*c*) and *f* electrons. The *c-f* hybridization-derived electronic structure can be directly probed by the angle-resolved photoemission spectroscopy (ARPES). In this work, we focus on YbAl<sub>2</sub>, which is known as one of the prototypical valence fluctuation systems, with the Yb mean valence of +2.2 [1]. Thus, YbAl<sub>2</sub> is a suitable system to investigate the *c-f* hybridized band structure in relation with the extremely strong valence fluctuations.

The ARPES experiment was carried out at the undulator beamline BL7U [2]. The single crystals of YbAl<sub>2</sub>, which were grown by the Lithium flux method, were cleaved *in situ* along the (111) plane. The Brillouin zone of YbAl<sub>2</sub> is shown in the Fig. 1. The total energy resolution and the measurement temperature were set to 20 meV and 12 K, respectively. The LDA band structure calculations were performed using the WIEN2k code.

Figures 2 (a)-(d) show the series of ARPES spectra and the ARPES intensity plot near the Fermi level along the  $\Gamma$ -K and  $\Gamma$ -M' directions, measured at  $h\nu=20$  eV [2]. The band dispersions obtained by the LDA calculation are also plotted in Figs. 2 (b) and (d). Their overall feature is well described in terms of the LDA calculation. In particular, the observed Yb  $4f_{7/2}$  band around the binding energy of 0.17 eV shows good agreement of energy with the calculation without any shift. This finding strongly suggests an extremely small renormalization in YbAl<sub>2</sub>. In the lower-binding energy region compared with the  $4f_{7/2}$  band, the anti-bonding bands of the *c-f* hybridization are clearly observed, responsible for the valence fluctuations in YbAl<sub>2</sub>. For the  $\Gamma$ -K direction, the position of the innermost band matches very well with that of LDA calculation. On the other hand, the experimental outer band has a slightly weaker dispersion. This band might not be separated from the more outer band, which does not cross the Fermi level as shown in the LDA calculation. For the  $\Gamma$ -M' direction, the experimental inner and outer bands are highly mixed, unlike those of the LDA calculation. The “mixed” band is located on the inside of the calculated ones and has almost same Fermi vector as the inner band in the  $\Gamma$ -K direction. This finding suggests that the inner Fermi surface is more circular than that of the LDA calculation [2].

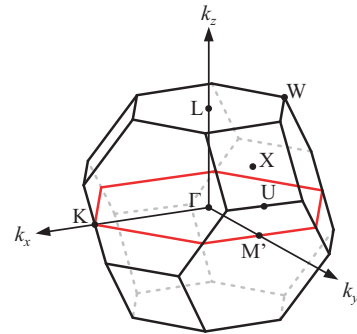


Fig. 1. Brillouin zone of YbAl<sub>2</sub>, in which  $k_z$  corresponds to the (111) direction of the fcc Brillouin zone. In the  $k_x$ - $k_y$  plane, the midpoint of the zone edge (K) is referred to as M' point, which is also equivalent to the midpoint between L and U points.

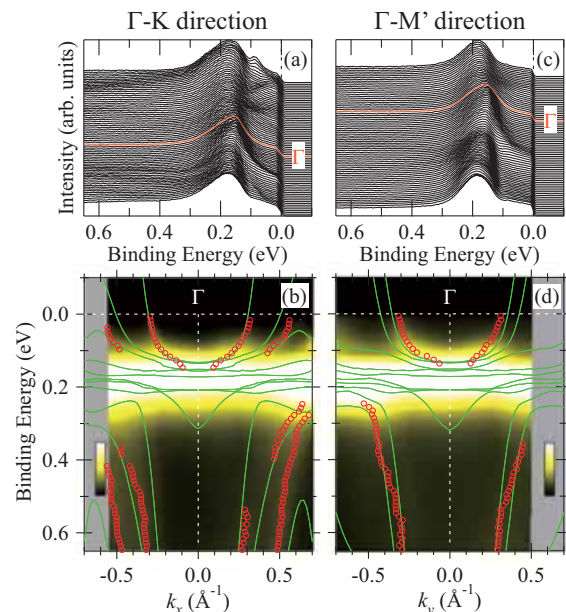


Fig. 2. (a) and (c) Series of ARPES spectra along the  $\Gamma$ -K and  $\Gamma$ -M' directions, respectively. (b) and (d) ARPES intensity plots of (a) and (c), respectively. The band dispersions obtained by MDC fitting (open circle) and LDA calculation are overlapped.

[1] M. Matsunami *et al.*, J. Phys. Soc. Jpn. **81** (2012) 073702.

[2] M. Matsunami *et al.*, Phys. Rev. B **87** (2013) 165141.

## Unique Fermi-Surface Topology Originated from Pt Atoms: An ARPES Study of the Electronic Structure of $\text{Ca}_{10}(\text{Pt}_4\text{As}_8)(\text{Fe}_{2-x}\text{Pt}_x\text{As}_2)_5$

X. P. Shen<sup>1</sup>, S. D. Chen<sup>1</sup>, Q. Q. Ge<sup>1</sup>, Z. R. Ye<sup>1</sup>, H. C. Xu<sup>1</sup>, F. Chen<sup>1</sup>, M. Xia<sup>1</sup>,  
B. P. Xie<sup>1</sup>, M. Matsunami<sup>2</sup>, S. Kimura<sup>2</sup> and D. L. Feng<sup>1</sup>

<sup>1</sup>State Key Laboratory of Surface Physics, Department of Physics, and Advanced Materials Laboratory, Fudan University, Shanghai 200433, People's Republic of China

<sup>2</sup>UVSOR Facility, Institute for Molecular Science and The Graduate University for Advanced Studies, Okazaki 444-8585, Japan

Recently, superconductivity up to 38 K was discovered in the novel iron-based superconductor  $\text{Ca}_{10}(\text{Pt}_4\text{As}_8)(\text{Fe}_{2-x}\text{Pt}_x\text{As}_2)_5$  [1]. In these compounds the metallic  $\text{Pt}_4\text{As}_8$  layer was introduced as a new intermediary layer, which distinguished them from other usual iron pnictides.

To study whether the  $\text{Pt}_4\text{As}_8$  layer contribute density of states (DOS) at the Fermi energy ( $E_F$ ) and estimate the strength of interlayer coupling between  $\text{Pt}_4\text{As}_8$  and  $\text{FeAs}$  layers, we have conducted angle-resolved photoemission spectroscopy (ARPES) studies on  $\text{Ca}_{10}(\text{Pt}_4\text{As}_8)(\text{Fe}_{2-x}\text{Pt}_x\text{As}_2)_5$  at beamline BL7U at UVSOR. The variable photon energies and polarizations enable us to successfully resolve the low-energy electronic structure and corresponding orbital characters in the 3-dimensional momentum space.

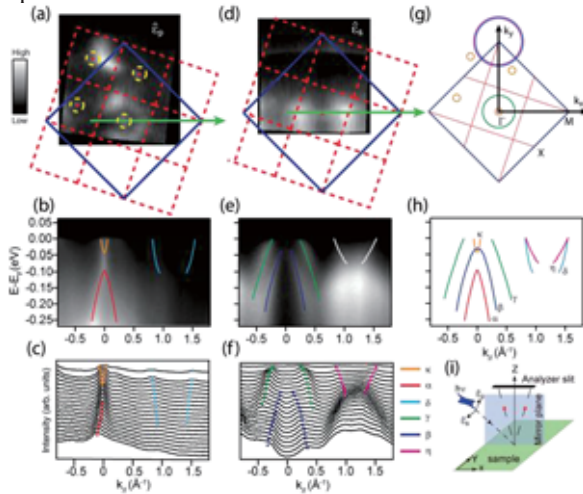


Fig. 1. The polarization-dependent ARPES data around  $\Gamma$  taken with 26 eV photons.

Figure 1 reveals the polarization dependent photoemission intensity maps and corresponding photoemission intensity plots along  $\Gamma$ -M. As shown in Fig. 1(a) and (b), the 2D blue BZ is from  $\text{FeAs}$  layer and the red dash one is from  $\text{Pt}_4\text{As}_8$  layer. The most remarkable feature here is that there are four small electron pockets ( $\kappa$ ) arranged around the zone centers of the  $\text{Pt}_4\text{As}_8$  BZs, as enclosed by the dash lines in Fig. 1(a), which is very likely from Pt atoms as proposed in the recent first-principles calculation[3]. Besides, we resolved two hole-like bands ( $\alpha$ ,  $\beta$ ), one hole pocket ( $\gamma$ ) around the zone

center and two electron pockets ( $\delta$ ,  $\eta$ ) around the zone corner, which show good correspondence to the electronic structures of other prototype pnictides and could be attributed to the  $\text{Fe-}3d_{xz}$ ,  $-3d_{yz}$ , and  $-3d_{xy}$  orbitals, respectively [3].

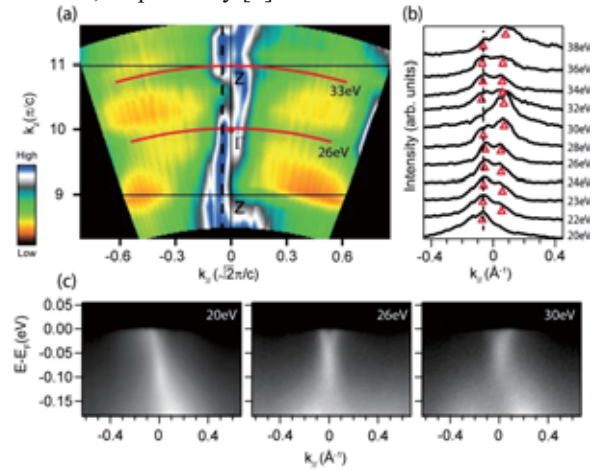


Fig. 2. The Fermi surface as a function of  $k_z$  in the  $p$  geometry.

Further  $k_z$  dependence of the  $\kappa$  electron pocket is shown in Fig. 2. The intensity distribution of the  $\kappa$  band shows a periodic variation in Fig. 2(a) if we take the inner potential to be 13 eV. By tracing the MDC's at  $E_F$  at each  $k_z$  [Fig. 2(b)], we could conclude that the  $\kappa$  electron pocket shows weak dispersion along the  $k_z$  direction.

In general, our data demonstrate that the Pt atoms indeed provide DOS at  $E_F$  and the  $\kappa$  electron pocket may participate in superconductivity in this novel material. However, the interlayer coupling between  $\text{Pt}_4\text{As}_8$  and  $\text{FeAs}$  layers is considerably weak according to the rather two-dimensional electronic structure and absence of obvious hybridization between  $\kappa$  and  $\alpha$  bands. Our results might open up new avenues for the exploration of high- $T_c$  superconductor by tuning the interlayer coupling between  $\text{FeAs}$  layer and additional metallic-like intermediary layers.

[1] N. Ni *et al.*, Proc. Natl. Acad. Sci. USA **108**, E 1019 (2011).

[2] H. Nakamura *et al.*, Physica C **484** (2013) 39.

[3] Y. Zhang *et al.*, Phys. Rev. B **83** (2011) 054510.

## Circular Dichroism ARPES Studies on Dresselhaus Effect in Non-Magnetic Semiconductors

W. Jung<sup>1</sup>, S. Cho<sup>1</sup>, Y. Kim<sup>1</sup>, B. Kim<sup>1</sup>, Y. Koh<sup>1</sup>, M. Matsunami<sup>2</sup>, S. Kimura<sup>2</sup> and C. Kim<sup>1</sup>

<sup>1</sup>*Institute of Physics and Applied Physics, Yonsei University, Seoul, Korea*

<sup>2</sup>*UVSOR Facility, Institute for Molecular Science, Okazaki 444-8585, Japan*

GaAs and InSb have been studied by many researchers and received attention. One of the issues in studying these semiconductors is the band splitting at the  $\Gamma$ -point. GaAs and InSb have a zinc blende structure and such materials have three hole bands that belong to the bulk band at the  $\Gamma$ -point. It is known that band splitting is due to the inversion symmetry breaking in the bulk. We studied this phenomena in light of the Dresselhaus effect.

Semiconductors with zinc blende and Wurtzite structures with a bulk inversion asymmetry such as ZnTe, ZnSe, CdS, CdSe, GaAs and InSb have been theoretically studied within a tight-binding model [1]. The effective one-body Hamiltonian with Dresselhaus effect is:

$$H = H_0 + H_D$$

$$H_D = \gamma[\sigma_x k_x(k_y^2 - k_z^2) + \text{cyclic permutations}]$$

Here,  $H_D$  is the Hamiltonian for the Dresselhaus effect,  $\sigma$  Pauli matrix, and  $\gamma$  the material dependent spin-orbit coupling constant. GaAs and InSb have a strong spin-orbit coupling and consequently show the Dresselhaus effect [2].

Topological insulators have strong spin-orbit coupling and have been studied in our group. According to our recent results, the orbital angular momentum (OAM) plays an important role in the formation of a Rashba-type surface band splitting [3]. We expect that OAM also greatly affects the electronic structure of semiconductors such as GaAs and InSb and that one should be able to obtain key evidences for the role of OAM in the Dresselhaus-type bulk band splitting. It was also recently reported that OAM can be measured by Circular Dichroism ARPES (CDARPES) [4, 5]. Therefore, we tried to study the OAM effect on the Dresselhaus effect by using circular and linear dichroism ARPES.

GaAs and InSb single crystals were purchased as wafer. ARPES measurement was performed at the beam line 7U of UVSOR-III. Crystals were cleaved *in-situ* at room temperature and the chamber pressure was better than  $5 \times 10^{-11}$  Torr. ARPES spectra were acquired with a hemispherical photoelectron analyzer (MBS A-1). We used linearly polarized as well as left and right circularly polarized (LCP and RCP) photons of 9–21 eV photons to avoid signal from the surface states.

Figure 1 shows ARPES data from GaAs. It is confirmed that GaAs has two hole bands at the  $\Gamma$ -point.

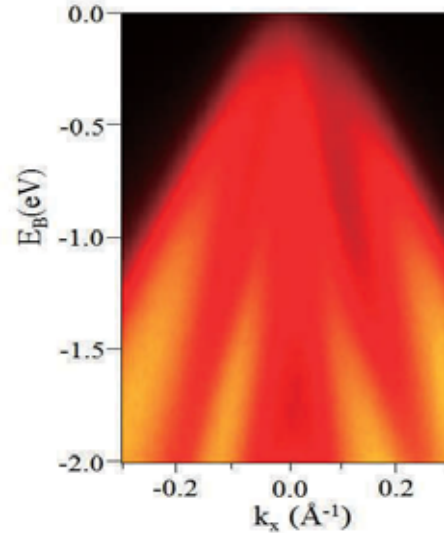


Fig. 1. ARPES image from GaAs (110) bulk state measured with linearly polarized 21 eV photon. The image is taken along the  $k_y = 0$  line.

To obtain the evidence for the Dresselhaus effect in ARPES, we performed CDARPES experiments on the GaAs and InSb with circularly polarized 9 eV photons, because the Dresselhaus effect gives a 30 symmetry in the CDARPES  $(I_{LCP} - I_{RCP}) / (I_{LCP} + I_{RCP})$ . However, we could not reach the  $\Gamma$  point with low-energy photons owing to the limitation of the beamline. It is expected that three-dimensional bulk band structure of GaAs and InSb gives us new information. Therefore, we will perform the three-dimensional ARPES to obtain the complete bulk electronic structure.

[1] W. T. Wang *et al.*, Appl. Phys. Lett. **91** (2007) 082110.

[2] J. W. Luo *et al.*, Phys. Rev. Lett. **102** (2009) 056405.

[3] S. R. Park *et al.*, Phys. Rev. Lett. **107** (2011) 156803.

[4] B. Y. Kim *et al.*, Phys. Rev. B **85** (2012) 195402.

[5] J. H. Park *et al.*, Phys. Rev. B **85** (2012) 195401.

## Temperature-Dependent Dispersive In-Gap State of The Kondo Semiconductor $\text{SmB}_6$

H. Miyazaki<sup>1,2</sup>, T. Hajiri<sup>2,3</sup>, M. Matsunami<sup>2,4</sup>, T. Ito<sup>3</sup>, S. Kunii<sup>5</sup> and S. Kimura<sup>2,4</sup>

<sup>1</sup>Nagoya Institute of Technology, Nagoya 466-8555, Japan

<sup>2</sup>UVSOR Facility, Institute for Molecular Science, Okazaki 444-8585, Japan

<sup>3</sup>Nagoya University, Nagoya 464-8603, Japan

<sup>4</sup>The Graduate University for Advanced Studies (SOKENDAI), Okazaki 444-8585, Japan

<sup>5</sup>Tohoku University, Sendai 980-8578, Japan

Samarium hexaboride ( $\text{SmB}_6$ ) is one of typical Kondo semiconductors/insulators with a valence fluctuation between  $\text{Sm}^{2+}$  ( $4f^6$ ) and  $\text{Sm}^{3+}$  ( $4f^5$ ) ions [1]. The electrical resistivity decreases on cooling, like a metal, above the temperature of 100 K, and then reveals a semiconductor-like character with activation energy of 15 meV, but the resistivity saturates below 20 K [2]. Though the origin of the constant resistivity at low temperatures has not been resolved for a long time, recently this behavior has been suggested to originate from metallic behavior at the edge state on the surface [topological Kondo insulator (TKI)] [3]. To clarify the origin of the anomalous electrical resistivity behavior of  $\text{SmB}_6$ , we performed three-dimensional angle resolved photoemission spectroscopy (3D-ARPES) to determine the electronic band structure directly.

A  $\text{SmB}_6$  (001) single crystal was cleaned by  $\text{Ar}^+$  ion sputtering and 1400 °C annealing cycles in the ultrahigh vacuum chamber with a base pressure of  $\sim 2 \times 10^{-8}$  Pa. Clean surface of  $\text{SmB}_6$  with the  $2 \times 1$  and  $1 \times 1$  (001) patterns was confirmed by a low energy electron diffraction method and no contamination, such as carbon, was observed by an Auger electron spectroscopy. The 3D-ARPES measurements were performed at the beamline 7U of UVSOR-III. The total energy and momentum resolutions for the ARPES measurement were set to 13 meV and  $0.006 \text{ \AA}^{-1}$  at the  $\Gamma$  point ( $h\nu = 26 \text{ eV}$ ) and 12 meV and  $0.003 \text{ \AA}^{-1}$  at the X point ( $h\nu = 10.6 \text{ eV}$ ), respectively.

Figure 1 shows the temperature-dependent ARPES spectra divided by the Fermi-Dirac distribution curve along the X–M line. At  $T = 40 \text{ K}$ , the  $k$ -dependence of the peak at  $E_B = 15 \text{ meV}$ , marked by open circles, is almost flat. The band becomes slightly dispersive at temperature below 20 K, i.e., the  $c$ - $f$  hybridization gap opens near the X point. At  $T = 10 \text{ K}$ , another band dispersion, with an electron pocket at  $k \sim 0.25 \text{ \AA}^{-1}$ , appears at  $E_B \sim 5 \text{ meV}$ , as shown by vertical lines. The dispersive in-gap state behavior suggests that the in-gap state is not a local state, such as an impurity state, but has the periodicity of the  $\text{SmB}_6$  unit cell. The ARPES data seem to be consistent with the electrical resistivity; i.e., the formation of the hybridization gap is visible above 20 K, while the in-gap state becomes dominant below 10 K. The band dispersion of the in-gap state is consistent with theoretical calculation [4, 5], i.e., the dispersive

in-gap state suggests the existence of an edge state. To determine the origin of the in-gap state, further studies are intended.

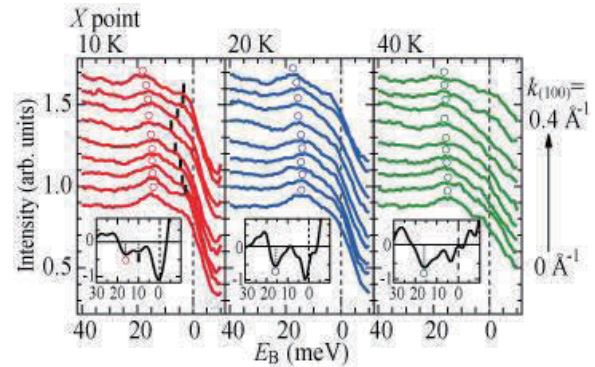


Fig. 1. Temperature dependence of ARPES spectra divided by the Fermi-Dirac distribution curve along the X – M line. The hybridization band dispersions are shown by open circles, and the observed dispersion in-gap state is shown by vertical lines. Insets show the second derivative curves of the ARPES spectra at  $k_{(100)} = 0.25 \text{ \AA}^{-1}$ .

- [1] R. L. Cohen *et al.*, J. Appl. Phys. **41** (1970) 898.
- [2] T. Tanaka *et al.*, J. Appl. Phys. **51** (1980) 3877.
- [3] M. Dzero *et al.*, Phys. Rev. Lett. **104** (2010) 106408.
- [4] M. Dzero *et al.*, Phys. Rev. B **86** (2012) 075105.
- [5] F. Lu *et al.*, arXiv: 1211.5863.

# High-Resolution ARPES study of $\text{Sn}_{1-x}\text{In}_x\text{Te}$ : Implication to Topological Superconductivity

T. Sato<sup>1</sup>, Y. Tanaka<sup>1</sup>, K. Nakayama<sup>1</sup>, S. Souma<sup>2</sup>, T. Takahashi<sup>1,2</sup>, S. Sasaki<sup>3</sup>, Z. Ren<sup>3</sup>,  
A. A. Taskin<sup>3</sup>, K. Segawa<sup>3</sup> and Y. Ando<sup>3</sup>

<sup>1</sup>Department of Physics, Tohoku University, Sendai 980-8578, Japan

<sup>2</sup>WPI Research Center, Advanced Institute for Materials Research, Tohoku University, Sendai 980-8577, Japan

<sup>3</sup>Institute of Scientific and Industrial Research, Osaka University, Ibaraki, Osaka 567-0047, Japan

Topological insulators (TIs) are a novel quantum state of matter where the bulk band gap induced by a strong spin-orbit coupling leads to the appearance of unusual gapless edge/surface states protected by time-reversal symmetry [1, 2]. The discovery of TIs triggered the search for their superconducting (SC) analogues, topological superconductors (TSCs). TSCs are accompanied by gapless Andreev bound states inside the SC gap which are often comprised of Majorana fermions. Very recently, point-contact spectroscopy revealed that indium-doped tin telluride ( $\text{Sn}_{1-x}\text{In}_x\text{Te}$ , called In-SnTe here) is possibly a new type of TSC [3]. This result is particularly intriguing in view of the fact that SnTe was recently elucidated to be materializing a new type of topological state called topological crystalline insulator (TCI) [4, 5] associated with topologically-protected surface states that emerge due to a combination of band inversion and mirror symmetry [4, 5]. It is thus of great importance to experimentally clarify the electronic states of In-SnTe relevant to the possible occurrence of topological superconductivity.

In this study, we have performed high-resolution angle-resolved photoemission spectroscopy (ARPES) of In-SnTe. By utilizing the low energy and variable photon energy ( $h\nu$ ) characteristics of the beamline BL7U, we have succeeded in directly observing topological surface state [6].

To clarify the effect of indium substitution on the electronic states of SnTe, we paid particular attention to the momentum space around the  $\bar{X}$  point of the surface Brillouin zone [Fig. 1(a)], because the topological surface states appear in this momentum region in SnTe [5]. Figures 1(b) and (c) represent a direct comparison of near- $E_F$  ARPES intensity between pristine and In-doped SnTe measured along a  $\mathbf{k}$  cut crossing the  $\bar{\Lambda}$  point. In SnTe, we observed a highly dispersive holelike band which is attributed to an admixture of the bulk and surface states with dominant contribution from the surface state near  $E_F$ , as confirmed by the  $h\nu$  independence. While the overall dispersive feature is significantly broader in In-SnTe, it is still possible to extract an intrinsic band dispersion for In-SnTe by taking second derivatives [see Fig. 1(d)]. The result of such an analysis clearly shows a linearly dispersive holelike band approaching  $E_F$ , which is similar to what is found in pristine SnTe. This result demonstrates that the topological surface state is likely to be present in In-SnTe. This

conclusion is further supported by the observation of the “M”-shaped band dispersion along the  $\bar{\Gamma}-\bar{X}$  cut [Fig. 1(e)], which can be regarded as a fingerprint of the Dirac-cone surface state of a TCI [5] where the calculated bulk-band structure never shows any M-shaped dispersion near  $E_F$ .

The present experiments elucidate that the bulk band inversion, which makes SnTe a TCI, is kept unchanged in In-SnTe. This band inversion and our observation of the topological surface state in In-SnTe assure that this material provides a fertile ground for the study of TSC [6].

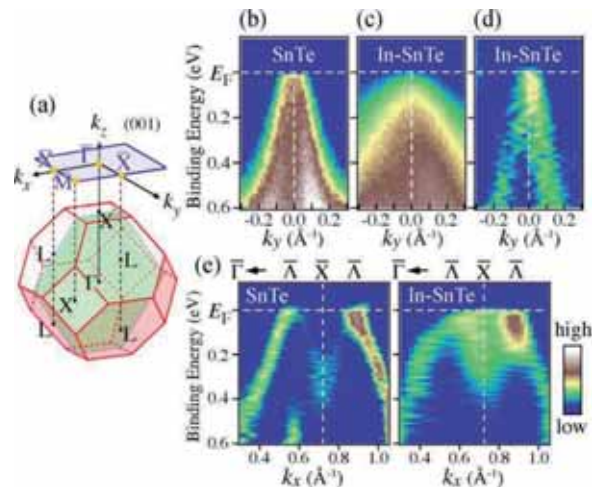


Fig. 1. (a) Bulk fcc Brillouin zone and corresponding tetragonal (001) surface Brillouin zone. (b) and (c) Comparison of near- $E_F$  intensity measured with  $h\nu = 21$  eV plotted as a function of  $k_y$  and binding energy across the  $\bar{\Lambda}$  point. (d) Second derivative of the data in (c). (e) Comparison of the band dispersion derived from the second derivatives of the MDCs along the  $\bar{\Gamma}-\bar{X}$  cut between pristine SnTe (left) and In-doped SnTe (right).

- [1] M. Z. Hasan and C. L. Kane, Rev. Mod. Phys. **82** (2008) 3045.
- [2] X.-L. Qi and S.-C. Zhang, Rev. Mod. Phys. **83** (2011) 1057.
- [3] S. Sasaki *et al.*, Phys. Rev. Lett. **109** (2012) 217004.
- [4] L. Fu, Phys. Rev. Lett. **106** (2011) 106802.
- [5] Y. Tanaka *et al.*, Nature Phys. **8** (2012) 800.
- [6] T. Sato *et al.*, arXiv:1212.5886.

## Temperature Dependence of Auger-Free Luminescence in $\text{Cs}_2\text{ZnCl}_4$

A. Ohnishi<sup>1</sup>, M. Kitaura<sup>1</sup>, M. Sasaki<sup>1</sup> and M. Itoh<sup>2</sup>

<sup>1</sup>Department of Physics, Yamagata University, Yamagata 990-8560, Japan

<sup>2</sup>Department of Electrical and Electronic Engineering, Shinshu University, Nagano 380-8553, Japan

In the present study, temperature dependence of Auger-free luminescence (AFL) in  $\text{Cs}_2\text{ZnCl}_4$  has been investigated in the temperature range  $T=15\text{--}300$  K. Experiments were performed at the BL-7B beam line of UVSOR. This report is one of results published in ref. 1.

Temperature dependence of emission spectra of  $\text{Cs}_2\text{ZnCl}_4$  were measured under photo-excitation at 21.4 eV. Typical results at several different temperatures are shown in a relative scale in Fig. 1. Three bands peaking at 3.3, 4.2 and 4.8 eV at 15 K are the AFL in  $\text{Cs}_2\text{ZnCl}_4$ , which come from radiative transitions between the Cl 3*p* valence band and the Cs 5*p* outermost-core band. On increasing the temperature, spectral widths of the 3.3 and 4.8 eV bands become broaden appreciably, while that of the 4.2 eV band is almost unchanged. This situation is clearly recognized in Fig. 2, where the full width at half maximum (FWHM) of the three bands is plotted as a function of temperature.

The existence of two AFL bands peaking at 4.2 and 4.8 eV is discussed. As shown in Fig. 2, when  $T$  is increased from 15 K, the spectral width of the 4.8 eV band indicates a remarkable broadening, while that of the 4.2 eV band is almost unchanged. Meanwhile, their decay times were identical to each other. It is, therefore, supposed that the difference in thermal broadening is attributed to the difference in the final state of the Auger-free transition, not the difference in the initial state. In this connection, it is worth noting that the 4.2 and 4.8 eV bands in  $\text{Cs}_2\text{ZnCl}_4$  are very similar in nature to the AFL in CsCl [2], in which two bands at 4.5 and 5.2 eV are also ascribed to radiative transitions between the Cl 3*p* valence band and the Cs 5*p* outermost-core band. For CsCl, Fukaya *et al.* [3], have theoretically studied the temperature dependence of AFL spectra by an extended deformable cluster model, which is based on a supposition that a core hole self-traps weakly by inducing lattice deformation around itself. Their theoretical study gives a satisfactory agreement with the experimental observation. By referring to their arguments, we consider on the existence of two AFL bands at 4.2 and 4.8 eV as follows. The high-energy band at 4.8 eV comes from the Auger-free transition of a self-trapped core hole to a localized state in the valence band due to an attractive potential of lattice deformation created in the initial state. The final state of the low-energy band at 4.2 eV, on the other hand, is an extended state in the valence band without lattice deformation. It is also supposed that the lattice relaxation of core holes may

play an important role for the 3.3 eV band, because this band becomes broadened significantly with increasing the temperature.

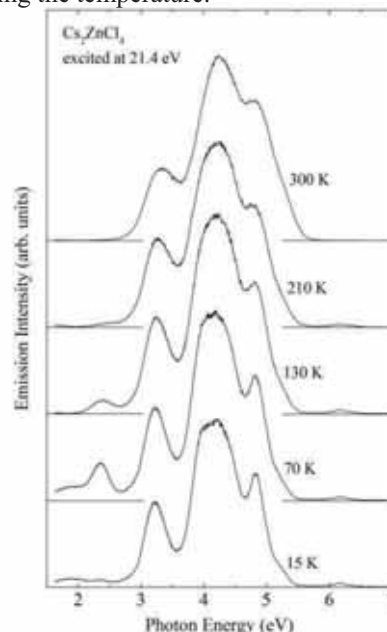


Fig. 1. Emission spectra measured at  $T = 15, 70, 130, 210$  and  $300$  K under photo-excitation at 21.4 eV.

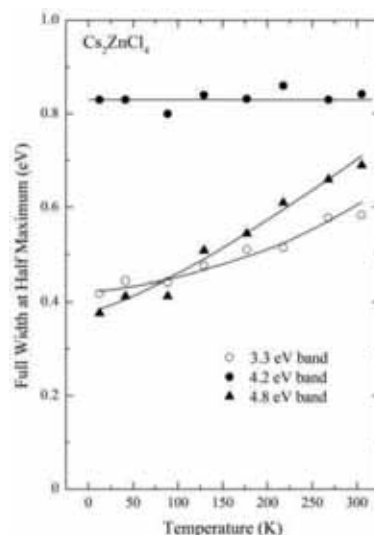


Fig. 2. Temperature dependence of the FWHMs of the 3.3, 4.2 and 4.8 eV bands.

[1] A. Ohnishi, M. Kitaura, M. Itoh and M. Sasaki, J. Phys. Soc. Jpn. **81** (2012) 114704.

[2] M. Itoh, M. Kamada and N. Ohno, J. Phys. Soc. Jpn. **66** (1997) 2502.

[3] M. Fukaya, Y. Kayanuma and M. Itoh, J. Phys. Soc. Jpn. **71** (2002) 2557.

## Luminescence of CsCl Heavily Doped with CsI

N. Ohno and K. Sakae

Graduate School of Engineering, Osaka Electro-Communication University, Neyagawa, Osaka 572-8530, Japan

Stimulation in iodine absorption bands of dilute  $\Gamma$ -doped alkali chlorides produces characteristic luminescence bands under excitation with UV light or with X-rays at low temperatures. These luminescence bands have been well explained in terms of localized relaxed excitons at  $\text{ICl}^-$  molecule ( $\Gamma^-$  monomer) and a complex of two iodine ions ( $\Gamma^-$  dimer) [1, 2]. However, optical and luminescence properties of heavily iodine-doped alkali chloride crystals have not been examined sufficiently for applying to high efficient scintillation materials. The present report describes the results of CsCl heavily doped with CsI.

The crystals of CsCl:I were grown by the Bridgeman method from reagent grade CsCl added with an appropriate amount of CsI (up to 3 mol%). The photoluminescence and photoexcitation spectra were measured at BL7B station. The photoluminescence spectra excited with photons near the exciton absorption region of CsCl were almost the same as those of the previous studies [3, 4]: two luminescence bands peaking at 3.92 eV (monomer) and 5.12 eV (dimer) at 15 K. Figure 1 shows the photoexcitation spectra for the monomer (blue) and the dimer emission (red) for 3 mol% CsCl:I. The excitation spectrum for the monomer is quite similar with that for the dilute case [3]. However, the spectrum for the dimer band is found to show a quite different behavior with heavily doped crystals [4]. This clear low energy tail of the excitation band for the dimer emission suggests that there coexist dimers, trimers and larger sizes of  $\text{I}^-$  ions (CsI cluster) in heavily-doped CsCl:I crystal as can be found in heavily-doped KCl:I [5].

The luminescence energies of the trimers and clusters of  $\text{I}^-$  ions in heavily doped CsCl:I crystals are expected to be different from that of  $\text{I}^-$  dimers. We have examined the dimer emission spectra excited at various photon energies. The results are shown in Fig. 2. It is clearly confirmed that the peak energy of the dimer band moves towards the low energy side when excited with photons of lower energy. Therefore, the luminescence bands are supposed to be the composite bands due to radiative annihilation of the relaxed exciton at dimers, trimers and clusters of  $\text{I}^-$  ions [5].

In CsCl crystals containing CsI above 1 mol %, there exists a small amount of dimer centers as compared with monomers, and moreover the amount of trimers and clusters of CsI is extremely smaller than those of monomers and dimers. The present results suggest that the excitons trapped in CsI clusters in heavily doped CsCl:I crystals would give the high luminescence efficiency.

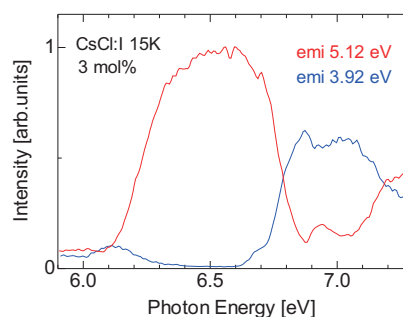


Fig. 1. Photoexcitation spectra of CsCl:I (3 mol%) crystal for the monomer (blue) and dimer (red) bands.

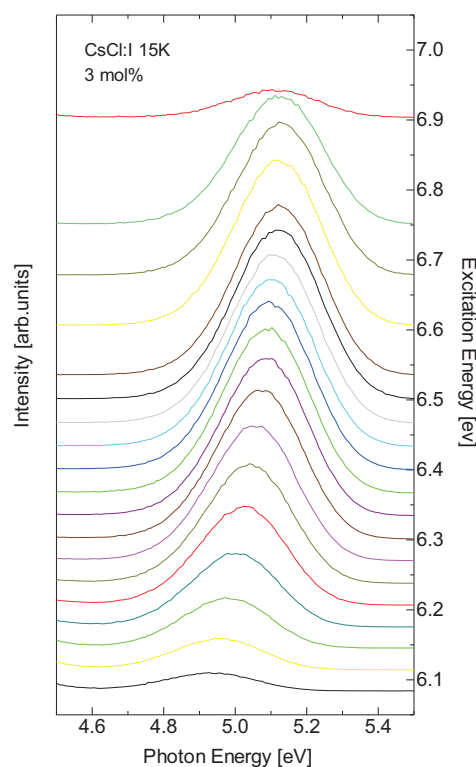


Fig. 2. Luminescence spectra of CsCl:I (3 mol%) crystal excited with photons of various energies ranging from 6.08 to 6.90 eV.

- [1] N. Nagasawa, J. Phys. Soc. Jpn. **27** (1969) 1535.
- [2] K. Kan'no, K. Tanaka and T. Hayashi, Rev. Solid State Sciences **4** (1990) 383, and references therein.
- [3] M. Yoshida and N. Ohno, Proc. Int. Conf. on Excitonic Processes in Condensed Matter (1996) 231.
- [4] N. Ohno and A. Ohno, UVSOR Activity Report **38** (2012) 83.
- [5] A. Ohno and N. Ohno, Phys. Status Solidi C **8** (2011) 112.

## Electronic Structure of the ZnO Treated by Microwave

K. Yoshida<sup>1</sup>, T. Sonobe<sup>2</sup>, H. Zen<sup>1</sup>, K. Hachiya<sup>2</sup>, K. Okumura<sup>1</sup>, K. Mishima<sup>1</sup>, M. Inukai<sup>1</sup>,  
H. Negm<sup>1</sup>, M. Omer<sup>1</sup>, Y.-W. Choi<sup>1</sup>, R. Kinjo<sup>1</sup>, T. Kii<sup>1</sup>, K. Masuda<sup>1</sup> and H. Ohgaki<sup>1</sup>

<sup>1</sup>Institute of Advanced Energy, Kyoto University, Gokasyo, Uji, Kyoto 611-0011, Japan

<sup>2</sup>Graduate School of Energy Science, Kyoto University, Yoshida-honmachi, Sakyo-ku, Kyoto 606-8501 Japan

Microwave (MW) heating is considered as an advanced method for a material processing, since it has several unique advantages such as rapid and selective heating over conventional methods. To date, several approaches have been investigated. For example, K.M Parida and S. Parija achieved the enhancement of a photocatalytic activity of ZnO by irradiating the ZnO with MW [1]. In addition, the activity as a catalyst of MgO in chemical reaction was also improved by irradiating the MgO catalyst with MW [2]. In this way, MW heating is considered as a one of useful techniques for improving properties of the functional materials. However, the change of the physical property, especially electronic structure, by MW irradiation has not been clarified well. The clarification of the effect of MW irradiation on electronic structure is important for design of materials such as photocatalyst, solar cells or material processing. Therefore, we investigated the electronic structure of the material treated by MW.

The photoluminescence was measured for the analysis of the electronic structure. BL7B was used as the light source and photon energy was changed from 2.92 eV (425 nm) to 3.54 eV (350 nm). A CCD array cooled by liquid nitrogen was used as the detector. The exposure time was 10 s. The measurement temperature was room temperature. Two types of ZnO were prepared. One was sintered at 873 K for 2 hours and not irradiated with MW. The other was sintered at 873 K for 2 hours and irradiated with MW of 500 W for 10 minutes. The treatment method of MW irradiation is shown in the reference [3].

Figure 1 is the photoluminescence spectra of ZnO with the MW irradiation. The sharp peaks from 1.5 eV to 1.8 eV and from 2.5 eV to 3.7 eV are the second order diffraction light of light source and fundamental excitation light, respectively. A broad band whose peak energy is 2.4 eV was observed.

In addition, the black and red dots in Fig. 2 show the PLE (photoluminescence excitation) spectra for the intensity of photoluminescence at 2.4 eV from ZnO with and without MW irradiation. In Fig. 2, the peak intensity of ZnO without MW irradiation is seen constant in any excitation energy. In contrast, in the case of the ZnO with MW irradiation, the intensity of the broad band peaks showed strong dependency on the excitation photon energy. The maximum intensity was observed at excitation energy of 3.21 eV. The black arrow in Fig. 2 shows the band gap energy (3.27 eV) of ZnO. From these results, it is considered

that a new energy band was created at lower energy than the conduction band by MW irradiation, and the excitation and relaxation process of electron was changed by the effect of the new energy band. As the conclusion, we found that the MW irradiation made significant change of the electronic structure of ZnO.

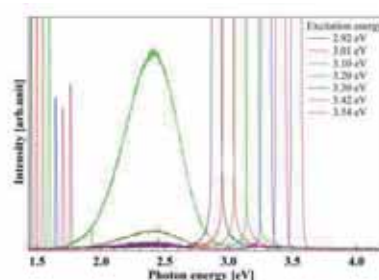


Fig. 1. Photoluminescence spectra of ZnO with MW irradiation.

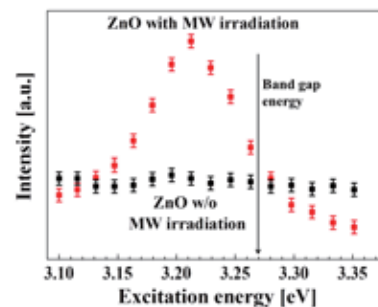


Fig. 2. PLE spectra of the intensities at 2.4 eV from ZnO with and without MW irradiation.

- [1] K. M. Parida, *et al.*, *Solar Energy* **80** (2006) 1048.
- [2] H. Mirzaei, *et al.*, *Chin. J. Catal.* **33** (2012) 1502.
- [3] T. Sonobe, *et al.*, *Jpn. J. Appl. Phys.* **49** (2010) 080219.

## Ultraviolet Photoelectron Spectra of Lu Encapsulated Fullerenes (I)

T. Miyazaki<sup>1</sup>, R. Sumii<sup>2,3</sup>, H. Umemoto<sup>4</sup>, H. Okimoto<sup>4</sup>, T. Sugai<sup>4</sup>, H. Shinohara<sup>4</sup> and S. Hino<sup>1</sup>

<sup>1</sup> Graduate School of Science and Engineering, Ehime University, Matsuyama, 790-8577, Japan

<sup>2</sup> Institutes for Molecular Science, Okazaki, 444-858, Japan

<sup>3</sup> Research Center for Materials Science, Nagoya University, Chikusa-ku, Nagoya, 464-8602, Japan

<sup>4</sup> Graduate School of Science, Nagoya University, Chikusa-ku, Nagoya, 464-8602, Japan

Fullerene cages encapsulate single as well as multiple metal atoms, metal nitrides and metal-carbides. Encapsulated metal atom(s) donate electrons to the cage, and affect the electronic structure of the fullerene cage [1, 2]. The amounts of the transferred electrons depend on the entrapped species and the fullerene cages. Recently, Lutetium atom(s) and lutetium-carbide encapsulated C<sub>82</sub> fullerenes, Lu@C<sub>82</sub> (I), Lu<sub>2</sub>@C<sub>82</sub> (II), Lu<sub>2</sub>@C<sub>82</sub> (III), Lu<sub>2</sub>C<sub>2</sub>@C<sub>82</sub> (II) and Lu<sub>2</sub>C<sub>2</sub>@C<sub>82</sub> (III) have been isolated. The NMR study revealed their cage symmetry, C<sub>2v</sub> (82:9) for Lu@C<sub>82</sub> (I), Lu<sub>2</sub>@C<sub>82</sub> (II) and Lu<sub>2</sub>C<sub>2</sub>@C<sub>82</sub> (II), C<sub>3v</sub> (82:8) for Lu<sub>2</sub>@C<sub>82</sub> (III) and Lu<sub>2</sub>C<sub>2</sub>@C<sub>82</sub> (III). In the current work, the UPS of Lu@C<sub>82</sub> (I), Lu<sub>2</sub>@C<sub>82</sub> (II), Lu<sub>2</sub>@C<sub>82</sub> (III), Lu<sub>2</sub>C<sub>2</sub>@C<sub>82</sub> (II) and Lu<sub>2</sub>C<sub>2</sub>@C<sub>82</sub> (III) will be presented and validity of the empirical rule is examined. Ultraviolet photoelectron spectra were measured at BL8B2 of Ultraviolet Synchrotron Orbital Radiation Facility of Institute for Molecular Science. The measured UPS were referenced against the Fermi level (E<sub>F</sub>) of gold deposited on the sample disk before the measurements.

The valence band UPS of Lu@C<sub>82</sub> (I), Lu<sub>2</sub>@C<sub>82</sub> (II) and Lu<sub>2</sub>C<sub>2</sub>@C<sub>82</sub> (II) obtained with  $h\nu = 20-55$  eV. Their onset energy (E<sub>onset</sub>) are 0.25 eV (Lu@C<sub>82</sub> (I)) and 0.64 eV (Lu<sub>2</sub>@C<sub>82</sub> (II) and Lu<sub>2</sub>C<sub>2</sub>@C<sub>82</sub> (II)), which are much smaller than that of empty C<sub>82</sub> (1.2eV). These are the results of electron transfer from the entrapped species to the cage. These fullerenes are semi-conductive. There are several structures labeled  $\alpha - \delta$  and A - E in the UPS of Lu@C<sub>82</sub> (I), Lu<sub>2</sub>@C<sub>82</sub> (II) and Lu<sub>2</sub>C<sub>2</sub>@C<sub>82</sub> (II). The UPS of Tb@C<sub>82</sub>, Er@C<sub>82</sub> and Y<sub>2</sub>C<sub>2</sub>@C<sub>82</sub> all of them have the same C<sub>2v</sub> symmetry are also shown in Fig. 4. Remarkable difference among these UPS is observed in the 9-11 eV region. While there is only one structure labeled  $\epsilon$  is observed in the UPS of Tb, Er, Y<sub>2</sub>C<sub>2</sub> entrapped fullerenes, two structures labeled X and Y are observed in the UPS of Lu entrapped fullerenes. The ionization energies of Lu 4f<sub>7/2</sub> and 4f<sub>5/2</sub> levels of Lu metal are 7.5 eV and 8.9 eV, respectively. Binding energies of X and Y are ranging from 9.3-9.8 eV and 10.8-11.2 eV, respectively, and they are much higher than those of Lu metal atoms by 2.0-2.5 eV. Further, energy separation between structures X and Y is 1.4-1.5 eV, which coincides with that of Lu4f<sub>7/2</sub> and Lu4f<sub>5/2</sub>. Thus, structures X and Y might be due to entrapped Lu atom(s). This could be the first observation of the photoelectrons of entrapped species in the ultraviolet photoelectron spectroscopy.

The UPS of Lu<sub>2</sub>C<sub>2</sub>@C<sub>82</sub> and Y<sub>2</sub>C<sub>2</sub>@C<sub>82</sub> are almost identical but that of Lu<sub>2</sub>@C<sub>82</sub> shows slight differences from them. These differences might be attributed to the difference in the amounts of transferred electrons. Probably, the amounts of transferred electrons in Lu<sub>2</sub>@C<sub>82</sub> and Lu<sub>2</sub>C<sub>2</sub>@C<sub>82</sub> are so different that their electronic structure is modified differently. Lu4f<sub>7/2</sub> and 4f<sub>5/2</sub> levels may be helpful to estimate them. The oxidation state of entrapped Lu atom might be +3. Since Lu4f<sub>7/2</sub> and Lu4f<sub>5/2</sub> binding energies of Lu@C<sub>82</sub> and Lu<sub>2</sub>@C<sub>82</sub> are almost the same, the electronic configuration might be (Lu<sup>3+</sup>)<sub>2</sub>@C<sub>82</sub><sup>6-</sup>. Possibly the original oxidation state of Lu atoms in Lu<sub>2</sub>C<sub>2</sub>@C<sub>82</sub> is +3, but entrapped C<sub>2</sub> might receive two electrons from them and hybridization or back donation takes place among Lu atoms and C atoms resulting Lu<sup>-3+ $\delta$</sup>  state.

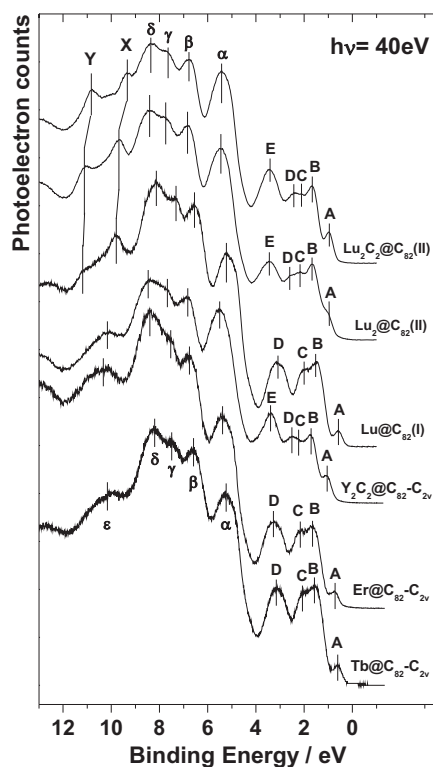


Fig. 1. UPS of endohedral fullerenes at  $h\nu = 40$  eV.

- [1] T. Miyazaki *et al.*, Chemical Physics **378** (2010) 11.  
 [2] T. Miyazaki *et al.*, Chemical Physics **397** (2012) 87.